GICAL SOCIETY

MEMOIRS

OF THE

COLLEGE OF SCIENCE

KYOTO IMPERIAL UNIVERSITY

SERIES A

VOL. XVIII, NO. 4

JULY 1935

KYOTO

Net Density of Starch

By **Bunsuke Takei**

(Received May 2, 1935)

Abstract

The net densities of starches are observed by applying the method of measuring densities by perfect evacuation. The density of purified starch of rice is found by measurement to be 1.646 and that of purified starch of potato 1.650. These are the greatest values hitherto observed.

In experiments recorded in a paper[1] previously published, U. Yoshida and the present writer measured the net density of ramie-cellulose by the method of perfect evacuation, and noted that the method can be well applied to any substances, powdery, fibrous or porous, which are liable to occlude gases and water. When the writer examined the starches of rice and potato by means of X-rays[2], the more reliable values of the densities of starches are required, as the differences between the lattice-forms of the starches of rice and potato seem to be fundamental even in the perfectly dry state. In this instance the writer applied the method of perfect evacution in measuring the net densities of starches in the same way as in the case of ramie-cellulose. Experimental details must be referred to the above-mentioned paper[3], while some results and discussions are shown below.

In preliminary experiments, the writer measured the densities of purified starches of rice and potato evacuated for various durations of time by heating at different temperatures in the bath of water or oil. The results of the experiments are shown in Figs. 1 and 2. In the case of Fig. 1 the time of evacuation was kept constant at 5 hours, and the temperature of the bath was varied between 10°C and 160°C. This temperature of the bath being taken as abscissa, the densities of purified starches of rice and potato are represented as ordinate in Fig. 1a; and the reduction of weight of the specimen by evacuation, which is represented as a percentage of the original weight of the unevacuated specimen dried in an ordinary "Adsol" dessicator, is taken as ordinate in Fig. 1b. In the case of Fig. 2 the temperature

1. U. Yoshida and B. Takei, These Memoirs, **15**, 1 (1932)
2. B. Takei: Jap. Jour. Phys., **8**, 85 (1933)
3. U. Yoshida and B. Takei: Loc. cit.

of the heating bath was kept constant at 50°C, and the time of evacuation was changed from 30 minutes to 10 hours. The time of evacuation is taken as abscissa in this case, and the ordinates in Figs. 2a and 2b have the same meanings respectively as in Fig. 1. From

Fig. 1 ○ for starch of rice × for starch of potato

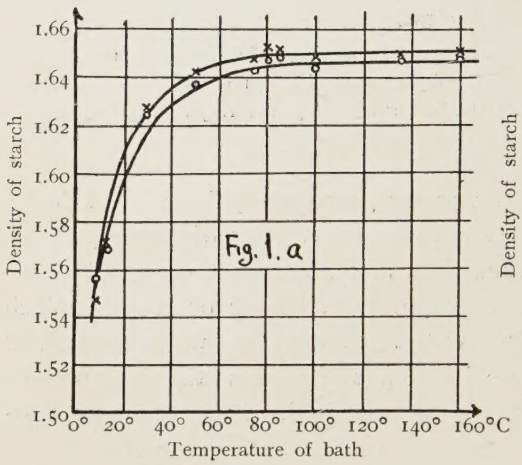

Fig. 2

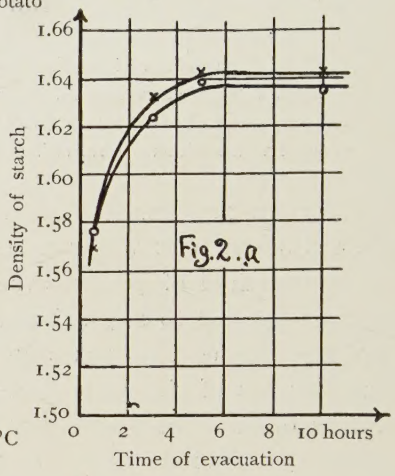

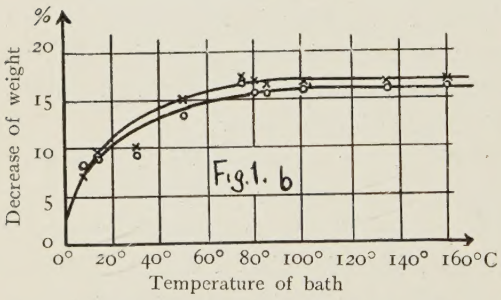

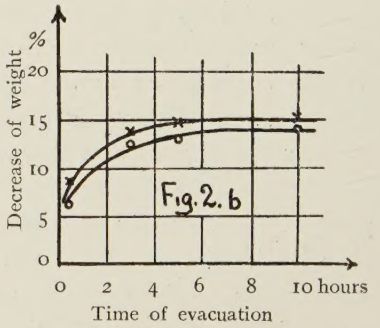

the curves thus represented in Figs. 1 and 2, we may conclude that the most suitable temperature of heating is between 70°C and 90°C, and that the convenient time of evacuation with the Cenco Hyvac pump is about 5 hours, for the densities and the reduction of weight remain unchanged at higher temperatures than 90°C and for longer times of evacuation than 5 hours It must be noted that when starches are heated to a temperature higher than about 100°C slight carbonization begins to take place and the specimen becomes yellowish.

By taking the various precautions before stated, the measurements of the most reliable densities of purified starches of rice and potato are

obtained. These are tabulated in Table I. The quantity of the specimen used in this case was from 2 gms. to 5 gms; and the probale error of the measurements was about ±0.2 percent. The mean density of the purified starch of rice is 1.646 and that of the purified starch of potato is little greater, viz. 1.650. As the density of rice starch was in every experiment observed to be a little smaller than that of the potato starch, this small difference of the densities of the two kinds of starches does not appear to be due to mere experimental errors.

Table I. Net Densities of Starches and their Decrease of Weight by Evacuation

Evacuation		Net densities		Decrease of weight in %	
Temperature	Time	Rice starch	Potato starch	Rice starch	Potato starch
75°C	5 hours	1.642	1.647	16.72	16.76
80°C	5 hours	1.647	1.653	15.55	16.73
85°C	5 hours	1.648	1.651	15.49	16.55
Mean values		1.646	1.650	15.92	16.55

So far as the writer is aware, the values of the densities of purified starches obtained by him are the highest observed hitherto for starches. For example, in the standard tables of physical and chemical constants the density of starch is tabulated as 1.50[1] and 1.56[2]. The reason why the writer's values are larger than those tabulated in the ordinary tables will be easily understood from the fact that the weights of the starches contained in the "Adsol" dessicator decreased by perfect evacuation, by about 16 percent of the original weight in the dessicator, as shown in the last column of Table I.

As will be seen in Figs. 1 and 2, the weight of the specimen decreases with evacuation in parallel with the increase in its density. This seems to be mainly due to the expulsion of water occluded in the specimen, for the colour of the electric discharge through the Geissler tube, connected in parallel with the glass tube containing the specimen, is the same as that peculiar to hydrogen gas. Thus assuming that the reduction in weight by evacuation is entirely due to the extraction of liquid water adhering to the specimen, the writer calculated the densities of the unevacuated specimens from the experimental data of Table I. These calculated values correspond fairly

1. International Critical Tables 2. Smithsonian Physical Tables

satisfactorily with the values obtained by evacuating the specimens for about 40 minutes by cooling them in a freezing mixture so as to prevent the extraction of liquid water from the specimen as far as possible. This will be seen clearly by comparing the data tabulated in Table II. Such coincidence between the calculated and the measured values seems to justify the previous assumption that the reduction in weight of the specimen is mainly due to the expulsion of liquid water adhering to the specimen.

Table II. Calculated Densities of the Unevacuated Starches and the Densities measured by using Freezing Mixture

	Rice starch	Potato starch
Mean densities by perfect evacuation	1.646	1.650
Reduction in weight by perfect evacuation	15.92 %	16.55 %
Densities of unevacuated starch calculated from the above data	1.493	1.476
Densities measured by using freezing mixture	1.499	1.493

Here it must be remarked that the present experiment was performed on the assumption that the net density of starch does not suffer any appreciable change by its swelling in water. If there is any doubt on this point, it will be safer to measure the density of starch again by dipping it into some suitable liquid other than water. It would be interesting to measure the density of soluble starch or granulose by the method of perfect evacuation by immersing it in alcohol.

In conclusion, the writer wishes to express his sincere thanks to Prof. U. Yoshida for his kind guidance during the research. His hearty thanks are also due to Prof. K. Kondo of the Department of Agricultural Chemistry for furnishing all the test materials.

A Study of the Minor Fluctuation of the Atmospheric Pressure (III)

By **Tadao Namekawa**

(Received May 5, 1935)

Part II. Analysis of the Microbarograms (Continued)

Section III

Rapid Rise of the Barometric Pressure

1. Introduction

The phenomenon, " Crochets d'orage ", i. e. the peculiar shape of the barometric trace associated with a summer shower or a winter squall, is very familiar to meteorologists. Numberless inquiries and researches have been made on this subject, and, in connection, also, with the recently advanced " Polar front theory," various reports and fairly detailed, have appeared from many places in the world.

It is not the wish of the present writer to look into these. He will give, in what follows, only the results of his own investigations in the matter, as part of this microbarographical study, by citing examples of the rapid rise of the atmospheric pressure in times of a shower or a squall.

2. Typical Examples

Ex. 1. An example of " Local Shower." 16 h, 23rd Apr., 1921.

Reproduction of the microbarograms: Fig. 54. (Three simultaneous records) $\Delta p \fallingdotseq 2$ mm. Hg. $\Delta T \fallingdotseq -6°C$

Weather Chart: Fig. 55. Remarks: This is a typical of a local shower. It must be noticed here that, in addition to the main shower occurring at about 16h, a minor shower was experienced at about 11 h. 45 min. and 13 h. 45 min.. This fact seems to suggest the mechanism of generation of this kind of local shower.

Ex. 2. An example of " Winter Squall." 17 h. 8th. Nov., 1922.

Reproduction of the microbarogram: Fig. 56. $\Delta p \fallingdotseq 2.5$ mm. Hg. $\Delta T \fallingdotseq -4°C$ Weather Chart: Fig. 57.

Remarks: This is an example of the rapid pressure rise which accompanies the passage of a squall line belonging to the extratropical cyclone which often attacks our locality in winter. The rise occurred

(Microbarograms : $\frac{1}{2}$ of original size)

23rd. April. 1920.

Fig. 55

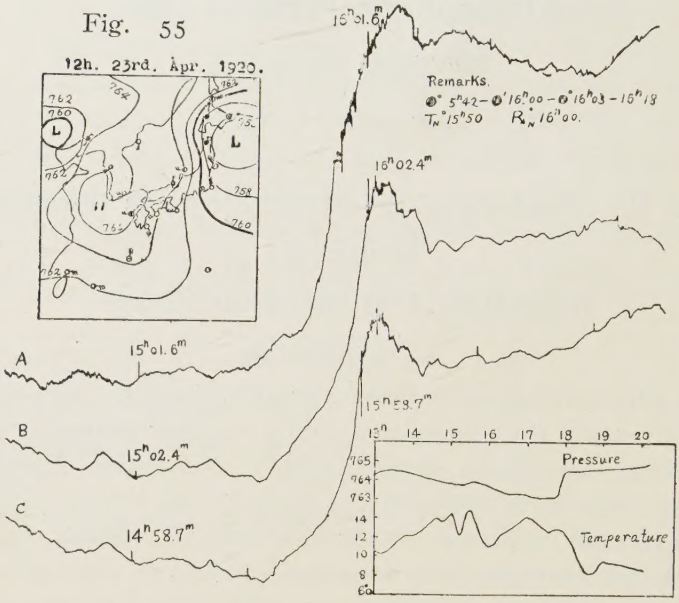

Fig. 54. Microbarograms at Kyoto.

Fig. 56. Microbarogram at Kyoto. ($\frac{1}{2}$ of original size)

8th. Nov. 1922.

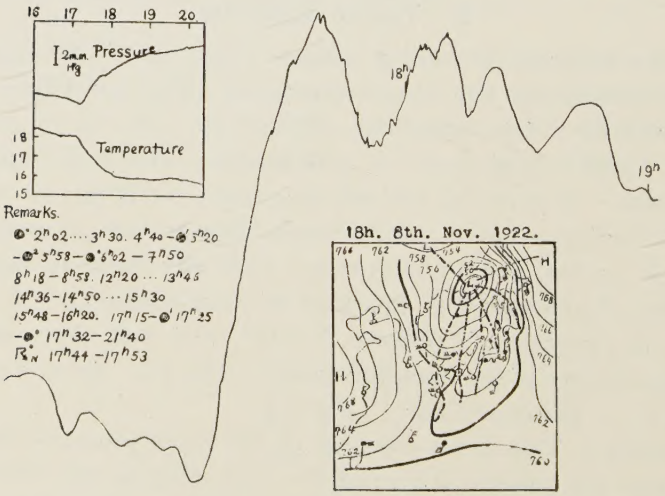

Fig. 57

when a warm south-easterly current suddenly gave way to a cold north-westerly current.

Ex. 3. An example of two different kinds of minor squalls. 6 h. 30 min., and 10 h. 45 min. 26th Apr., 1926.

Reproduction of the microbarogram: Fig. 58. Weather Chart: Fig. 59.

(Microbarogram : $\frac{1}{2}$ of original size)

Fig. 59

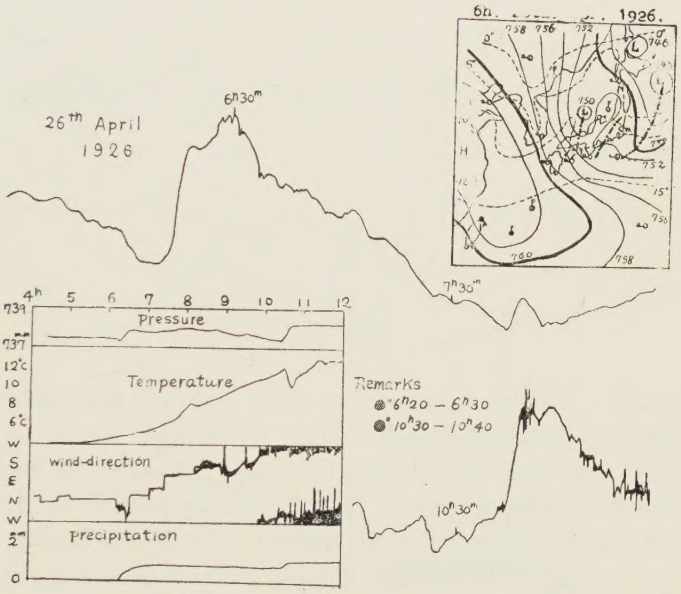

Fig. 58. Microbarogram at Kyoto.

Remarks: In Fig. 58 the minor squall which passed at 6 h. 30 min. was accompanied by slight rain of 0.3 mm. depth and a rapid rise of pressure of 0.7 mm. Hg., the air temperature showing no change.

But, later, at about 10 h. 45 min., another minor squall is shown to have passed; and, this time, a rapid rise of pressure of 0.7 mm. Hg., a sudden temperature fall of about 2°C., wind change from south to north, with suddenly increasing velocity, and rainfall of 0.2 mm. depth, were observed. These two minor squalls are presumably of the same structure, but the former did not present all the characteristics of normally recorded when a squall is passing. This can be accounted for by supposing that the first squall occurred in the upper strata of the atmosphere, thus partly eluding the observer on the ground. We shall hereafter call squalls of this type " Upper Squalls ", and ordinary

squalls, like that which came after in this example, " Surface Squalls ", in order to distinguish between the two kinds.

Ex. 4. An example of an " Upper Squall" 1 h., 25th May, 1929.

Reproduction of the microbarogram : Fig. 60. Weather Chart : Fig. 61.

(Microbarogram : $\frac{1}{2}$ of original size)

Fig. 60. Microbarogram at Kyoto.

Fig. 61

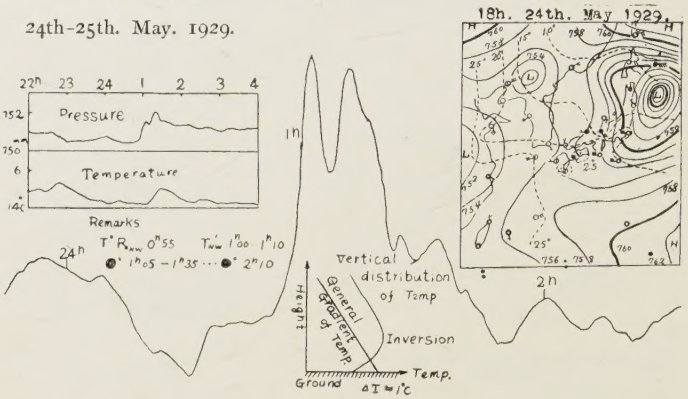

Fig. 62

Remarks : In this example, a quick rise of pressure of about 2 mm. Hg. is observed together with a thunder shower. The air temperature does not fall, but rises. This phenomenon can be explained fairly well by assuming that the squall passed over the thin surface air cooled by radiation at night in the Kyoto Basin. The air temperature rose, as in Fig. 62, when the surface layer was destroyed and the temperature distribution was restored to normal.

Among those which the writer calls " Upper Squalls " are included squalls, which, like this example, are only modified by the existence of a surface layer. Among them are also included, for convenience' sake, structural squalls, which have been made known and discussed by Bjerkness and his colleagues.

3. Detailed Examinations of Winter Squalls

Ex. 5. A squall at 23 h, 24th., Feb., 1922.

Reproduction of the microbarogram and meteorologrames at Kyoto, Kobe, and Osaka : Fig. 63.

Reproduction of the barograms and the thermograms at various stations : Fig. 64. Remarks on the squall : Table 8. Weather Chart at 18 h. 24th : Fig. 65. Weather Chart at 22 h. 24th and isochronous chart showing the advance of the squall : Fig. 66.

Fig. 63

(Microbarogram : $\frac{1}{2}$ of orininal size)

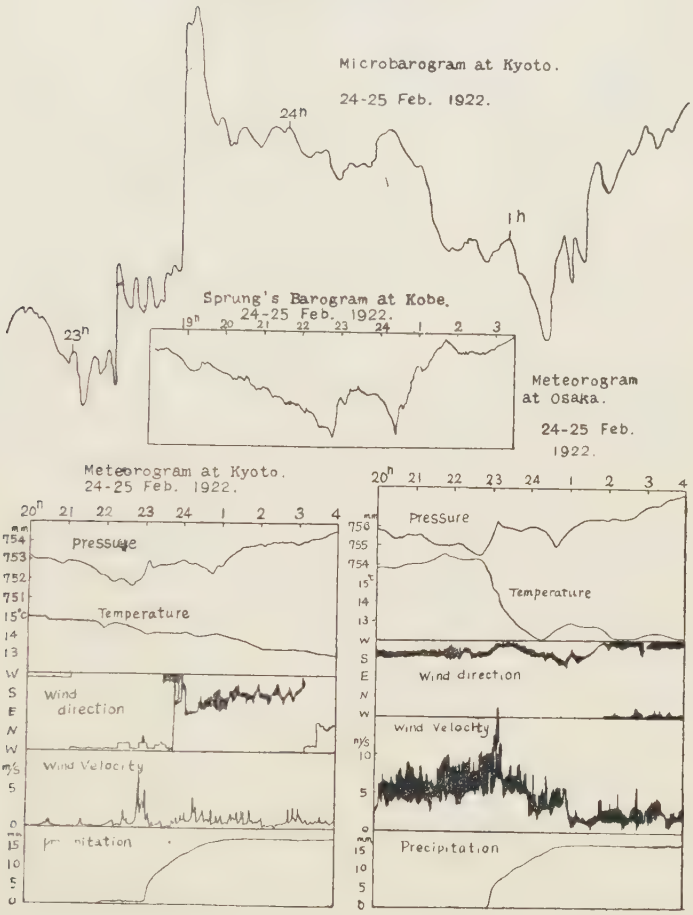

From Figs. 63, 64, 65, 66 and Table 8, it is clear that the squall travelled ESE. at a speed of about 60 Km/hour (17 m/s). Moreover, it is possible to conjecture from these records the probable structure of the squall as shown in Fig. 67. As this figure explains itself, no further comments are necessary. The only remaining question is the minor barometric trough appearing behind this squall. The barometric troughs appear with most squalls and are larger or smaller as the case may be. The writer first attributed this trough to the effect of a revolving fluid which occurs behind the head of the squall. But, in spite of most careful investigation, he could not find any trace of a revolving fluid passing with the squall. The key must be sought

Table 8

Stations.	Squall on 24th Feb., 1922			V-shaped depression behind the squall.		Meteorological Remarks.
	Passage time.	Prss. Change ΔP	Temp. Change ΔT	Passage time	Depth.	
Tadotu	21^h	1.8mm.	−5.5°C	23^h	0.6mm.	◎°18^h34−◎′19^h05−◎°20^h02−◎′20^h51−◎²$21^h04$−◎°22^h30−22^h55
Okayama	21^h10^m	1.8	Steady	22^h25^m	0.6	◎°17^h03−17^h45, ◎°18^h35−◎′20^h50−◎²$21^h10$◎′21^h13−◎°22^h50−23^h15. T′NW 21^h07−K′E 21^h34−
Murotozaki	22^h10^m	1.8	−3.0	0^h20^m	1.0	−<°SW−K°SW22^h20−, ◎°22^h30−, K°SSW22^h50→K°SE23^h05−23^h50, −◎°−1^h20
Tokusima	22^h		−3.0			◎°21^h43−◎′22^h07−◎°23^h20−23^h57
Kôbe	22^h50^m	1.3		0^h25^m	1.2	◎°21^h56−◎′22^h22−◎°22^h35−◎²$22^h49$−0^h40K′N23^h15−23^h43 ⁄23^h
Miyazu	22^h	2.0	gradual continuous fall			◎°7^h30−2^h35 (next day), 8^h10−8^h55
Wakayama	23^h	1.5	−4.0	0^h50^m	1.0	◎°21^h25−◎²$23^h30$−◎°23^h50−0^h50
Ôsaka	13^h10^m	1.8	−4.0	0^h50^m	1.2	◎°16^h18−◎′23^h02−◎²$23^h08$−◎′23^h25−◎°0^h28−, K′23^h15−23^h47
Yagi	23^h45^m	1.5	−2.0	1^h17^m	0.4	
Kyoto	23^h30^m	1.0	invisible fall	1^h10^m		◎°16^h55−17^h15, ◎°18^h32..21^h45 ◎°21^h54−◎′22^h33−◎°22^h34−◎′22^h48−◎°22^h55−◎′23^h03−◎²$23^h06$−◎′23^h12−◎²$23^h21$−◎′23^h23−◎²$23^h29$−◎°23^h35−◎′23^h47−◎°1^h05−1^h20…1^h53−2^h52 (25th). T8W23^h36−K°23^h37, K°23^h43. T°S23^h48−23^h52.
Hikone	23^h55^m	1.8	−4.5	1^h30^m	1.5	
Tu	0^h20^m	1.2	−4.0	2^h or earlier		◎4^h50−8^h10, 18^h40−5^h00 (next day) 8^h35−8^h53
Gihu	1^h or earlier	1.5	−3.5			◎°6^h58−7^h15, 8^h25−10^h50, ◎°22^h54−◎′23^h00−◎°2^h04−2^h37
Fukui	23^h10^m	2.0 not sudden	−3.5 not sudden			◎°22^h03−◎′22^h40−◎²$23^h15$−◎′24^h00−1^h15

Fig. 64

Fig. 66a
Weather Chart.

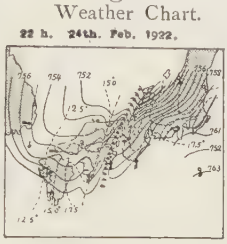

Fig. 66b

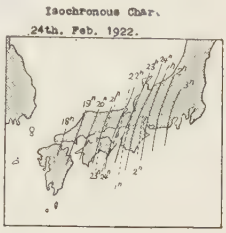

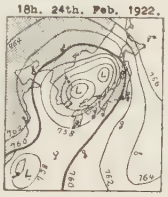

Fig. 65

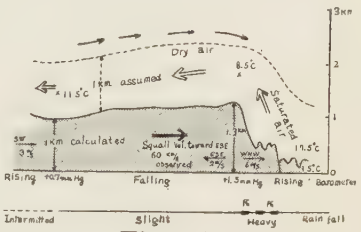

Fig. 67

elsewhere. The writer belives that the reason for this pressure-fall can be explained on the assumption that the squall head is covered by a warm current about 1 Km. deep, as shown in Fig. 67. He also believes that the wave-like pressure-disturbance observed after the passage of a squall is due to internal waves occurring on the boundary surface between cold and warm air.

Ex. 6. A squall at 6 h., 12th., Mar., 1925. Reproduction of the microbarogram, and the meteorolograms: Fig. 68 and Fig. 69.

Weather Chart at 6 h, 12th: Fig. 70. Remarks on the squall: Table 9. In this example are found the following four characteristic lines: (i) Line of sudden intrusion of warm current. (ii) Line of "Upper Front." (iii) Line of "Main Squall." (iv) Line of "Secondary Squall."

Remarkable phenomena to be noticed in this example are that, when the squall passes, the air temperature rises at Osaka, and a sudden rise of above 10°C is observed at the Yagi Observatory. This temperature rise is to be attributed to the passage of the so-called "Disguised Front", as is shown clearly in Fig. 71. About five hours before the first appearance of the squall i. e., approximately between 1 h. and 2 h. on that day, barometric waves with a period of about 8 min. are observed. This phenomenon had already been discovered by W. Schmidt, who says that, as these barometric waves occur from

Fig. 68
(Microbarogram ; $\frac{1}{2}$ of original size)

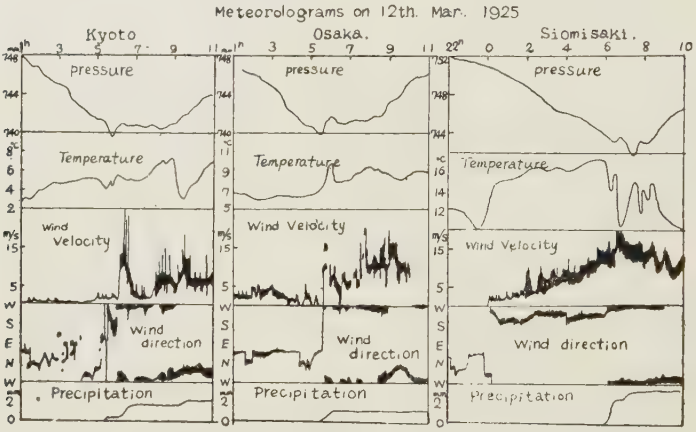

Fig. 69

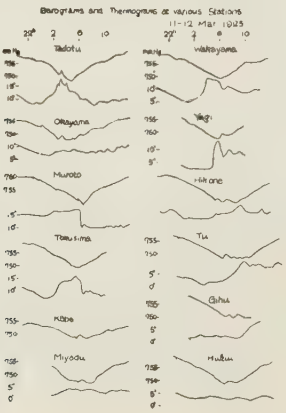

Fig. 70

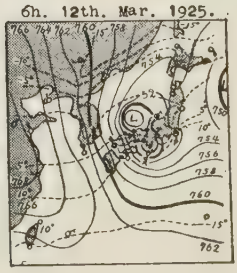

Table 9. (a) Penetration of warm Air. 12th Mar. 1925.

Stations	Time of passage	Change of temp. ΔT	Remarks.
Murotozaki	Before 22^h00^m 11th	4.0°C	NNE→SW
Sionomisaki	23^h50^m 11th	4.0°C	NNE→SW
Tadotu	2^h00^m or little later	6.0°C	
Tokusima	2^h00^m or little later	5.0°C	N→W
Wakayama	3^h30^m	5.5°C	
Yagi	4^h42^m	13.3°C	

Table 9. (b) Upper Squall. 12th. Mar. 1925.

Stations	Time of passage	Change of press. ΔP (in mm. Hg.)	Remarks
Okayama	3^h25^m	1.3	NE→NNW
Kôbe	4^h20^m		
Miyazu	4^h30^m not certain	0.5	
Ôsaka	5^h20^m		NE
Kyôto	5^h00^m		NW, Thunder SW. $4^h40^m-4^h57^m$
Hikone	5^h00^m or little later	1.0	
Gihu	6^h00^m or little later	1.0	Hail shower Thunder $5^h40^m-6^h50^m$
Hukui	6^h00^m	0.5	Rain moderate

Table 9. (c) Main Squall. 12th. Mar. 1925.

Stations	Time of passage	Change of press. ΔP (in mm. Hg)	Change of temp. ΔT (in °C)	Remarks
Sionomisaki	6^h00^m	1.2	−5.5	SW→W, Rain $6^h00^m-6^h20^m$, 2.5mm
Tadotu	4^h20^m	1.5	−4.0	Rain & thunder
Tokusima	5^h40^m	1.8	−5.0	SW→W, 10m/sec.
Wakayama	6^h00^m or little before		−3.0	
Yagi	6^h00^m	2.2	−4.3	
Okayama	4^h40^m	0.8		N→WSW, 10m/sec. Rain moderate
Kôbe	5^h35^m	2.1		Rain
Miyazu	5^h40^m	1.0		
Ôsaka	5^h50^m	1.8	−1.0	SW→WNW, 15m/sec. Rain
Hikone	6^h30^m	1.2		
Kyôto	6^h04^m	1.5	not fall	S→W Rain moderate
Tu	6^h40^m	1.9		
Gihu	7^h20^m	2.0		Rain slight

Table. 9. (d) Secondary Squall. 12th Mar. 1925.

Stations	Time of passage	Change of press. ΔP	Change of temp. ΔT	Remarks
Okayama	7^h20^m	1.8mm.	decrease	W→NW, 10m/sec
Kôbe	8^h45^m	2.0mm.		
Miyazu	8^h00^m	−2.0mm.	−2.0°C	
Ôsaka	8^h50^m	not remarkable	not remarkable	WSW→NW, 15m/sec
Kyôto	9^h15^m		−4.0°C	W→NW Rain slight
Hikone	9^h30^m	2.3mm. not sudden	−3.5°C	
Tu	9^h40^m	Steady	Steady	Rain feeble
Hukui	8^h50^m	Rising	Decreasing	Rain, snow, hail

Fig. 71

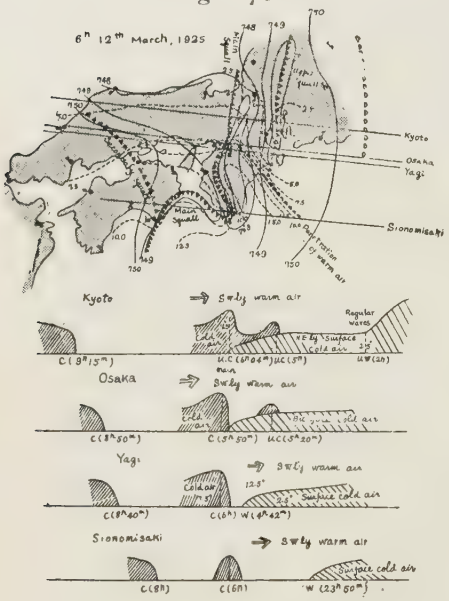

10 to 11 hours before a squall, it is possible to forecast a squall from them. But it seems to the present writer more natural to regard the waves as appearing near the warm front.*

Ex. 7. Example of regular barometric waves before a squall, 27th May, 1921. Fig. 72 shows that the squall passes Kyoto at 14 h. 30m., while the regular waves of pressure are recorded at about 11 h., i. e., about 3 hours before the passage of the squall. Fig. 73 is the weather chart of the day.

4. Statistical Study

The results of the statistical studies of noteworthy disturbance of this kind during the 11 years covering 1919—1929 are shown in Table 10.

* Met. Zs. **29** (1912) 406—412.

Fig. 72. Microbarogram at Kyoto.

(Microbarogram ; $\frac{1}{2}$ of original size)

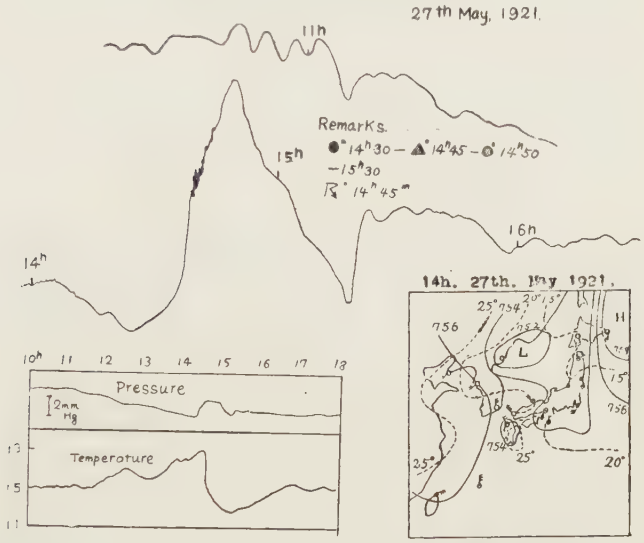

Fig. 73

Table. 10 Number of Occurrence of this Type.

Yearly Variation	No. of Occ.	Seasonal Variation	No. of Occ.	Daily Variation	No. of Occ.
1919	7	Jan.	2	oh—2h	2
1920	3	Feb.	9	2— 4	1
1921	18	Mar.	15	4— 6	4
1922	12	Apr.	10	6— 8	2
1923	8	May.	6	8—10	3
1924	8	Jun.	5	10—12	4
1925	3	Jul.	15	12—14	12
1926	9	Aug.	7	14—16	29
1927	10	Sept.	11	16—18	24
1928	8	Oct.	5	18—20	7
1929	8	Nov.	6	20—22	3
		Dec.	3	22—24	3
Total.	94		94		94

Barometer Rise (mm. Hg.)	No. of Occurrences	Temperature Fall. °C	No. of Occurrences
0.5—1.0	37	1.0	26
1.0—1.5	33	1.0—3.0	18
1.5—2.0	11	3.0—5.0	16
2.0—2.5	3	5.0—10.0	24
2.5—3.0	3	10<	1
uncertain	7	uncertain	9
Total.	94	Total.	94

Section IV

On the Disturbance-Type of the Microbarograms

1. Introduction

In the preceding three sections of Part II, abnormal types have been classified and discussed. These types, however, are recorded more frequently in association than in isolation. Therefore, when barometric waves, microbarographic depressions, etc. are recorded continuously in our microbarograms, they will, hereafter, be taken up, not analytically, but synthetically, and these records will be called "Disturbance-Type of the Microbarograms." Thus the microbarograms can be divided into two types —— Normal Type and Disturbance Type, the latter including all the abnormal types.

2. A Statistical Study of the Disturbance-Type of the Microbarograms

Fig. 74

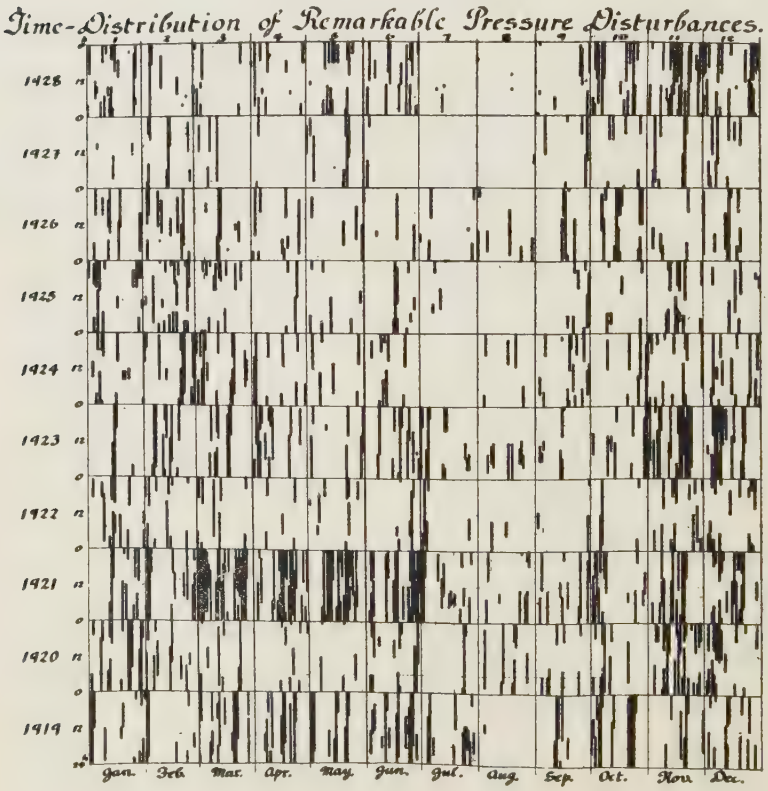

The time of the appearance of this type during the ten years covering 1919–1928 is shown in black line in Fig. 74. A coordinate system is adopted in this figure, with months (Jan.—Dec.) and hours (oh–23h) as abscissa and ordinate respectively, the years arranged vertically in their order. This figure forms the foundation of our statistical study. The ratio between the sum of the duration hours of

Fig. 75

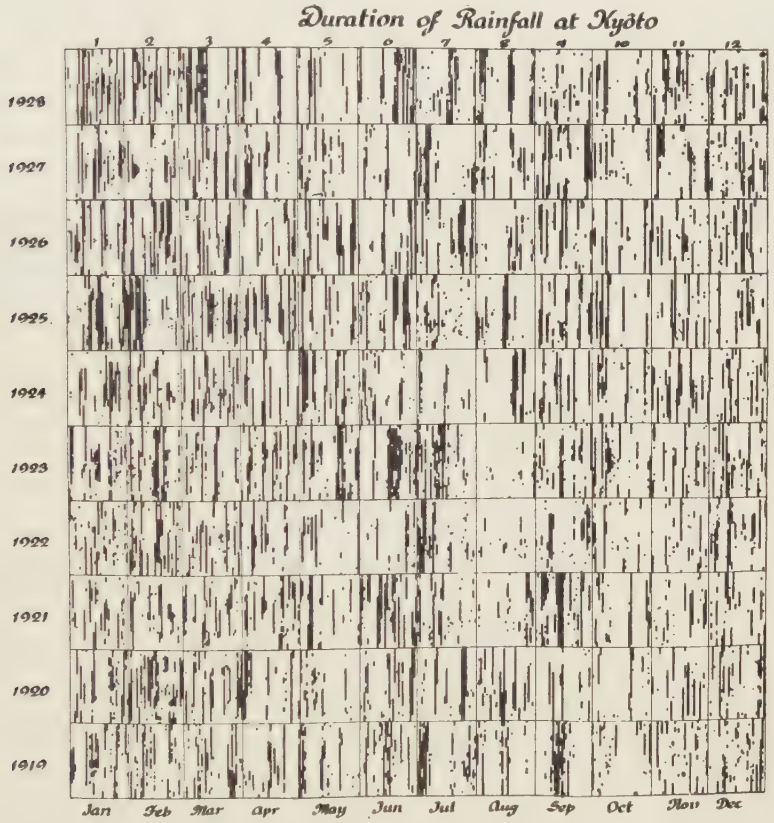

the occurrences of the disturbance type for day-time (6h–18h) and night time (18h–6h) is 44 : 56. The duration hours at night are longer in their total-sum. The statistics of the duration hours of this type are shown in Table 11, where D indicates the total hours of its occurrence within a particular year or month, and F, the number of its occurrences. Accordingly, " D/F " represents the mean duration hours of a single occurrence, and D/T, the ratio of the total hours of occurrences to the entire hours of a particular year or month. From

this table, the total hours of occurrences are found by calculation to be 12.8% of the total hours under investigation, and the average number of hours of a single occurrence proves to be 14.1 hours. D/T, which shows the seasonal variation, reaches maximum (21.0%) in November and minimum (4.0%) in August. On the whole, D/T is greater in the cold season, the period Oct.–Mar. having 58% and the period Apr.–Sept., 42%. That November and March have the greatest number of occurrences is due to the fact that in these months the alternation of the monsoon occurs; and *Baiu*, the rainy season of Japan, increases the number in June. Moreover, the occurrence of this type varies each year in frequency and time; D/T being maximum (25.7%) in 1921, minimum (5.9%) in 1927; the difference amounting to 20%, although these statistics cover only ten years. In order to investigate the relation between the occurrence of this type and rainfall, the duration-time of rainfall of Fig. 74 is substituted for that of the occurrence of Disturbance-Type. Thus we have Fig. 75. Here, this type is shown to appear most frequently in bad weather, but it is impossible to count

Table 11

		Jan.	Feb.	Mar.	Apr.	May	Jun.	Jul.	Aug.	Sept.	Oct.	Nov.	Dec.	Total	D/F	D/T
1928	D	124	62	38	69	98	134	8	2	47	164	246	180	1172		
	F	13	7	4	8	9	11	3	2	6	9	14	12	98	12.1	13.4
1927	D	14	82	53	10	76	14	2	5	61	26	96	80	519		
	F	3	10	6	2	6	2	2	3	5	3	3	8	53	9.8	5.9
1926	D	90	105	61	71	43	29	31	38	62	109	32	102	773		
	F	6	9	6	6	4	3	4	5	4	7	4	6	64	12.1	8.8
1925	D	88	119	79	32	32	36	10	3	48	31	104	55	637		
	F	9	14	11	4	6	7	3	3	6	5	10	8	86	7.4	7.3
1924	D	65	157	143	87	51	62	2	37	90	81	92	124	991		
	F	9	10	8	5	4	5	2	4	10	4	8	9	78	12.7	11.3
1923	D	47	128	113	144	72	138	115	61	39	104	267	200	1428		
	F	2	5	4	10	4	6	7	8	5	6	7	7	71	20.1	16.3
1922	D	134	69	79	32	52	40	50	15	19	46	128	82	746		
	F	12	9	9	4	8	5	4	2	4	3	9	10	79	9.5	8.5
1921	D	106	123	423	275	280	277	139	62	118	125	165	157	2250		
	F	6	6	12	10	8	9	12	5	7	9	7	11	102	22.0	25.7
1920	D	208	108	83	40	32	105	32	85	57	89	236	128	1203		
	F	9	9	6	7	5	9	3	6	8	5	14	12	93	13.0	13.7
1919	D	107	47	169	159	158	189	122	7	71	219	144	114	1506		
	F	7	4	10	7	4	11	9	1	3	6	4	6	72	20.9	17.2
Total	D	983	1000	1241	919	894	1024	511	315	612	994	1510	1222	11225		
	F	76	83	76	63	58	68	49	39	58	57	80	89	796		
D/F		12.6	12.1	16.4	14.6	15.4	15.1	10.4	8.1	10.5	17.4	18.9	13.7		14.1	
D/T%		132	14.2	16.7	12.6	12.0	14.2	6.9	4.2	8.5	13.4	21.0	16.4			12.8

it among the prognostic phenomena of rainfall. We next consider the relation between this type and the distribution of pressure. The distributions of pressure at the time of the occurrence of this type are roughly classified into ten groups in Fig. 76. The numbers of occurrences of disturbance types belonging to each of these ten are shown in Table 12. Table 13 shows the

Fig. 76

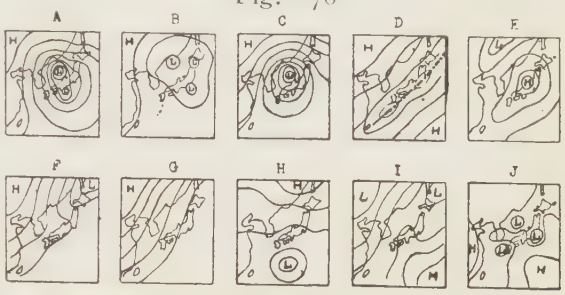

Table 12

Month / Type	Jan.	Feb.	Mar.	Apr.	May	Jun.	Jul.	Aug.	Sept.	Oct.	Nov.	Dec.	Total
A	18	20	18	9	12	17	5	0	8	12	19	22	160
B	7	6	3	13	13	17	14	8	9	4	8	11	113
C	14	11	16	6	4	9	6	12	11	4	11	10	114
D	6	13	16	20	11	5	0	1	6	14	13	12	117
E	9	11	8	13	14	15	1	7	17	18	14	11	138
F	10	14	7	0	3	1	0	1	3	2	13	17	71
G	10	7	6	1	0	0	0	0	0	1	3	9	37
H	1	2	1	1	0	0	5	4	6	2	1	0	23
I	0	0	0	0	0	3	12	1	0	0	0	0	16
J	1	0	1	0	0	1	4	4	1	0	0	0	12

Table 13

"A" — Groups of cyclones	20.0
"B" — Groups of minor cyclones	14.1
"C" — Single cyclone	14.2
"D" — Col-shaped isobar	14.6
"E" — Migratory anticyclone	17.2
"F" — Border of westerly type	8.9
"G" — Westerly type	4.6
"H" — Border of northerly type	2.9
"I" — Border of southerly type	2.0
"J" — Border of southerly type with several secondary cyclone	1.5

sums of the numbers in percentage. "A", "B" and "C", which are cyclonic, contain 48.3% of the whole number of occurrences.

"D" occurs during periods of monsoon alternation, and is observed frequently in spring and fall. "F" and "G" are seen in winter, and "H", "I" and "J" in summer. Here a doubt arises whether the converse of the result of the above statistical study is true i. e.— whether the pressure distributions described above are necessarily accompanied by disturbance-type of the microbarograms. The doubt is not endorsed by the facts. The statistics of the 3 years from 1926 to 1928 show that 42% of the cases of D group pressure distributions and a considerable percentage of the cases of the A, B, and C groups are accompanied by the disturbance-type of microbarogram. It may, therefore, be regarded as certain that, in cyclonic areas, minor fluctuations of pressure often recorded. A considerable percentage is also assigned to the cases of E group, which often gives rise to temperature inversions and is well-conditioned for the occurrence of atmospheric waves. It is almost the same with J group. The other groups have small percentage numbers. At any rate, the distribution of pressure alone cannot sufficiently account for these disturbance-types. The above result, of the statistical investigation of the relation between the pressure distribution and the microbarographic disturbances approximately agrees, in essentials, with the reports of several meteorologists on the same subject.*

3. Typical Examples

Ex. 1. 30th June–2nd July, 1923. Reproduction of the microbarogram and the meteorograms: Fig. 77. Weather Charts: Fig. 78. On the weather chart showing the pressure disturbance in fluctuation, the

Fig. 77 a

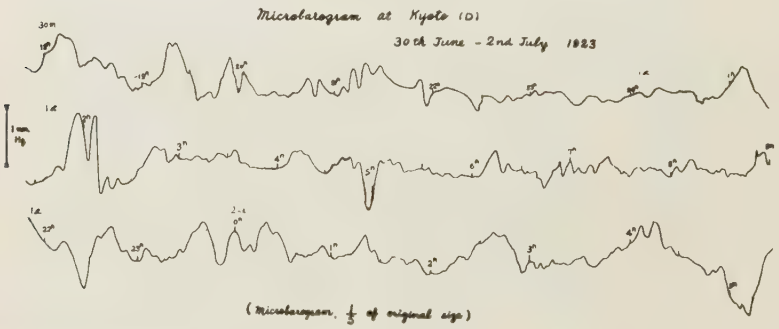

* Cave: "The Structure of the atmosphere in clear weather." P 78. Met. Mag., Feb. (1922) 1.; Clayton, Harvard Ann. XI appendix.

Fig. 77 b

Meteorolograms. 30th Jun.—2nd Jul. 1923.

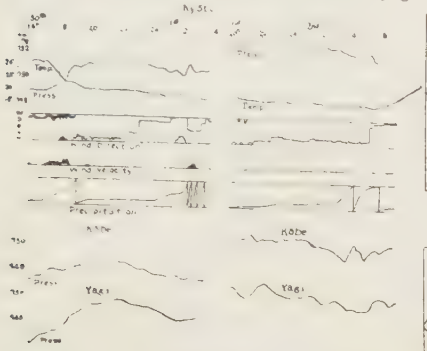

Fig. 78

Weather chart 30th Jun.—2nd Jul. 1923.

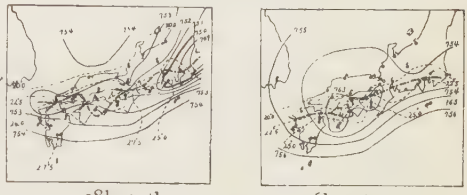

18h 30th 6h 1st

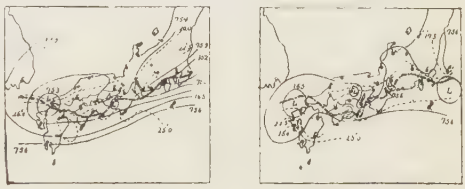

22h 30th 22h 1st

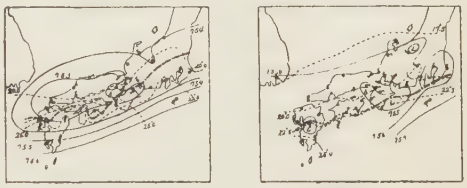

2h 1st 6h 2nd

west part of Japan is covered by a depression zone, and small secondary cyclones are found in many places. On the southern coast, warm southerly winds are blowing with considerable velocity. It is inferred from these facts that there is a warm current over a cold current. As is often stated, such a condition of atmospheric strata as this is favourable for the occurrence of barometric waves. While the fluctuation continues, the sky is clouded and a heavy rain falls now and then. During the rainfall, striking pressure disturbances are often, but not always, recorded. This example belongs to group D.

Ex. 2. 22nd–23rd Feb., 1924. Reproduction of the microbarogram and the meteorolograms: Fig. 79. Weather Chart: Fig. 80. This is one of the cases of group F. The border of a continental anticyclone passes near the southern coast of Japan proper. A newly-formed cyclone is seen near Chôshi.

According to J. Bjerkness, the juxtaposition of cold and warm currents is necessary for the formation of a cyclone. It is a necessary condition also for the occurrence of a pressure disturbance. So, where there is a striking pressure disturbance, as in this example, a newly-formed cyclone is often found.

Ex. 3. 5th Oct., 1928. Reproduction of the microbarograms: Fig. 81. Weather Chart: Fig. 82. This disturbance of pressure belongs

Fig. 79

(Microbarogram : $\frac{1}{3}$ of original size)

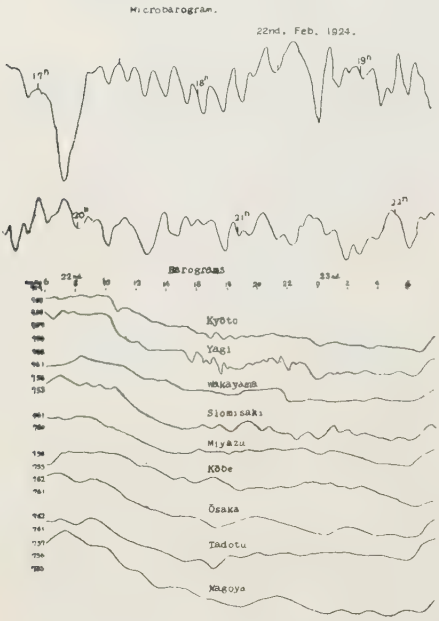

Fig. 80

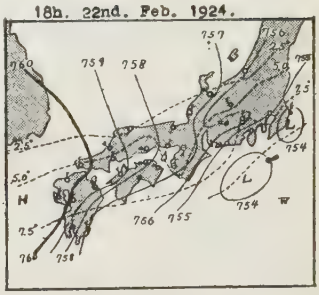

Fig. 82

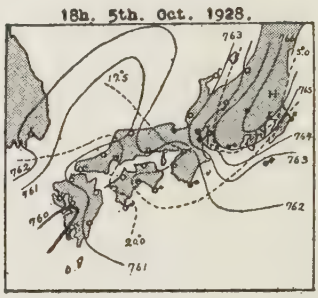

Fig. 84

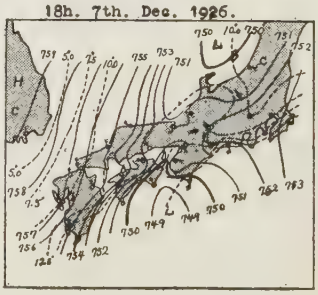

to group E. On the weather chart, a remarkable fluctuation of pressure is recorded in the tail of the eastward migratory anticyclone. This example is one of the most characteristic of disturbance-types, the amplitude of barometric waves being as large as about 0.5 mm. Hg., and the duration considerably long. The weather is cloudy, with a cold north-easterly wind blowing. But, on Mt. Ibuki, southerly wind and a dense fog are observed. These facts point to the existence of a rather powerful discontinuous surface. This fluctuation is recorded also by the microbarograph at Takayama, Gihu Prefecture. But nothing is recorded at Beppu in Kyûshû.

Ex. 4. 7th Dec., 1926. Reproduction of the microbarogram : Fig. 83. Weather Chart : Fig. 84. This is one of the cases of group D, and shows the fluctuation of pressure near a trough line of V-shaped depression. The discontinuous line is very distinctly traced on the weather chart, but it becomes an *Upper Front* in such

Fig. 81

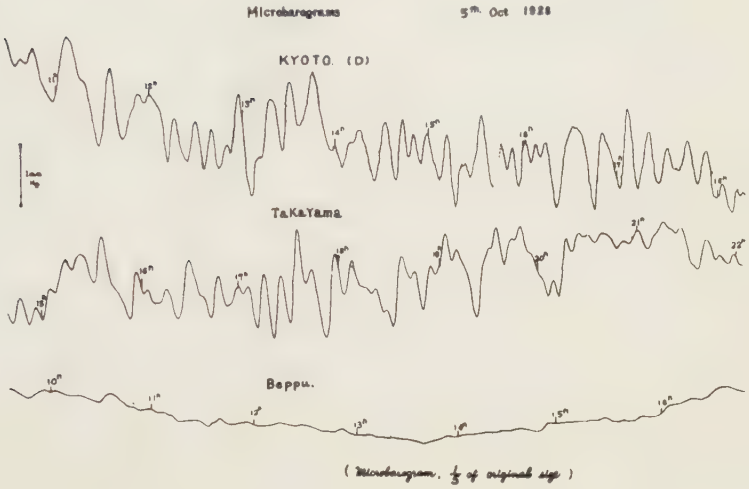

Fig. 83

(Microbarogram : ⅓ of original size)

inland places as Kyôto. The *Upper Front* passes Kyôto at about 16h and the barometric trough at about 18h. As this example shows, the neighbourhood of the trough line of the V-shaped depression is a region of striking pressure disturbance.

Section V

Some Interesting Miscellaneous Examples of the Microbarograms

1. On Two Examples of Fast Moving Disturbances of Atmospheric Pressure (Velocity, ca. 60. m.p.s.)

Shortly after 19h on the 28th Jan., 1928, and also shortly after 9h on the 5th Feb. in the same year, the microbarograph recorded remarkable pressure disturbances at Kyôto. (Cf. Fig. 85, and Fig. 87).

Fig. 85

(Microbarogram ; $\frac{1}{3}$ of original size)

accuracy cannot be expected, so that the curves of the front on the isochronous chart, have been obtained by smoothing down a little what resulted originally from actual records. At any rate, the velocity thus found is, on the 28th Jan., 66m/s from W to E, and, on the 5th Feb., 63m/s from WNW to ESE. Both of these velocities, which are almost equal, moved 2° of longitude in an hour, their direction being roughly from W to E. The pressure disturbance at the time can also be seen from the distribution of pressure on the weather chart. The peak and valley of the pressure disturbance

The records of these disturbances, taken at various other stations, have been collected and put in due order in Fig. 86, and Fig. 88. These traces of baromometric pressure are roughly of the same form, though there are slight differences. To ascertain the state of propagation, an isochronous chart is drawn by linking together the phase times of the minor barometric trough in the front of the sudden rise of barometric pressure. The time records of the self-recording barographs must be correct approximately, but absolute

Fig. 86

Barograms.

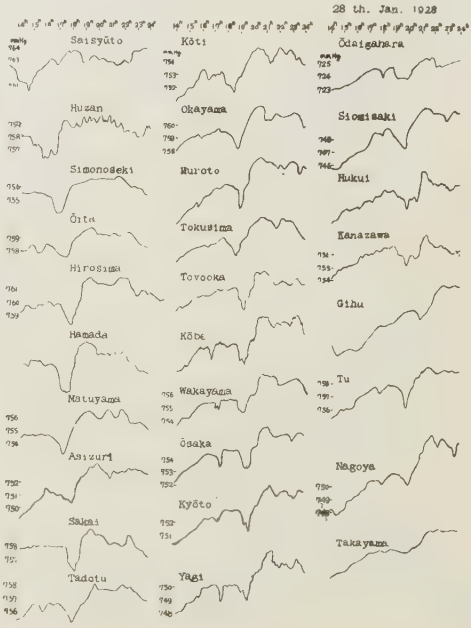

are situated as high and low pressures at points with a proportional distance between them. The problem gets clearer, when, as in Fig. 89, this disturbance and the general field of pressure are considered apart.

As the time of this disturbance, no striking fluctuations of meteorological elements are apparently observed; quite contrary to expectation, there is no change of wind-record. In the case of a rapidly propagating disturbance as in this example, however, it need not be deemed necessary that, the horizontal gradient of pressure $\frac{\partial p}{\partial x}$ should be great, even when the time rate of pressure change $\frac{\partial p}{\partial t}$ is large. Besides, if the influence of the friction near the surface of the earth is taken into consideration, the apparent scarcity of wind change is not surprising, though it must be accepted that the wind change is a little too scarce.

Fig. 87

(Microbarogram ; $\frac{1}{3}$ of original size)

Fig. 88

Barograms.

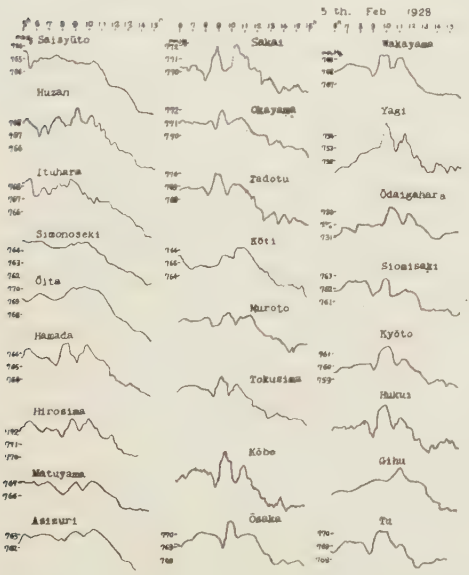

Now, the questions set before us are the cause of such a pressure disturbance and its velocity of propagation. It is impossible to guess the cause only from observations on the surface of the earth. The question of

Fig. 89

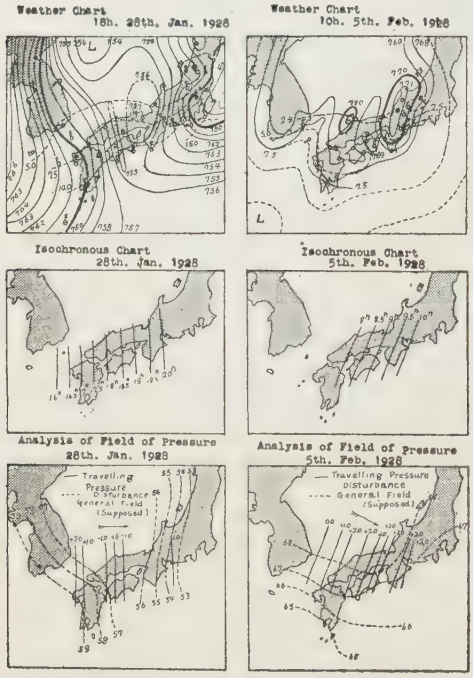

velocity seems to be equally difficult. The velocity of a cyclone or a squall is generally under 30m/s, and very rarely, if ever, reaches 60m/s. The present writer has never received a report of a pressure disturbance with a velocity of 60m/s. His attempt to solve this problem by applying some of the existing theories concerning the velocity of propagation of pressure disturbances has been fruitless. If, for example, in $V(\mathrm{m/s}) = 9.6\sqrt{P(\mathrm{mm.\ Hg.})}$, $\Delta P = 4$mm. Hg. we get 20 m/s, which differs greatly from 60 m/s. Again, in Bjerkness' formula, $C = 1.69\sqrt{(\theta' - \theta)(100 - P)}$, $\theta - \theta'$ is the value of the temperature spring on the discontinuous surface, and P is the value of the pressure there. This equation is to be regarded as a special case of the present writer's internal wave theory propounded in Part I. Of course, this equation applies when both strata are at rest, and a convective term must be added when they are in motion. Its value is not definite, and is 10 m/s at most. Thus in the above equation, if we take C=50m/s, we shall get a temperature gap of about 20°C for a height of the discontinuous layer of about 5 Km.; about 15°C for 7 Km.; and about 10°C for 10 Km. according to the table in his paper. If the height of the discontinuous layer is about 7 Km. with a temperature gap of 15°C., the overturn of the cold and warm air with the depth of 400 m. produces the pressure change of 2 mm. Hg. This is easier to explain. It is very doubtful, however, whether such a structure is really possible in so high a layer.

The following bold inference may here be propounded. In the first instance, the disturbance occurs at 19.5 h on the 28th Jan., and, in the second, at 9.1 h on the 5th Feb., the interval being 181.6 hours. The former travels a distance covering about 2° longitude in an hour, approximately along the latitude circle. Therefore, if it goes round

the earth at this speed, we have $2^\circ \times 181.6 = 363.2^\circ$ which is very near to 360°. This may be a mere coincidence, but too remarkable a coincidence to be lightly dismissed. From the physical point of view alone, it is a great strain on the imagination to think of an internal wave making its appearance after having travelled round the earth in more than a week. Whether this is fact or fiction could be quickly decided, if barograms were collected from all over the world and examined, though some difficulty may be experienced in such a procedure. The writer, therefore, cordially requests meteorologists who have chanced to read this paper to examine their barograms for any helpful information on this point and send their records of corresponding waves, if any such be found to exist.

2. Recurring Minor Squalls in the Basin of Kyôto

In late autumn and early winter, after the passage of a continental cyclone, when a north-westerly gale blows in the Kyôto Basin, several minor squalls are, not infrequently, experienced in succession. On such an occasion, a short rain or snow is immediately followed by a blue sky, which instantly gives way again to rain or snow. When this quick alternation has been repeated several times, the observer is apt to be bewildered. Such a phenomenon is called by the native inhabitants "*Kyôshigure*." Of course, there may be many more causes of "*Kyôshigure*" but that above mentioned is, without doubt, one of the causes. W. N. Shaw has also given his opinion on this kind of quickly recurring squalls.* Typical examples may be given to begin with.

Ex. Pressure disturbance of the 20th Feb., 1928. Fig. 90 shows minor squalls experienced at intervals of about one hour. From the meteorologrames in Fig. 91, the following characteristics are obtained :—

Temp :	min. →	increase →	max. →	decrease →	min. →	·····
Humidity :	max. →	decrease →	min. →	increase →	max. →	·····
Weather :	·····	fair ·····	rain ·····	fair···
Wind Vel. :	max. →	decrease →	min. →	increase →	max. →	·····
Pressure :	max. →	decrease →	min. →	increase →	max. →	·····

These characteristics are the same as those found when ordinary squalls are passing. The meteorologrames recorded at various places in the Kyôto Basin and the vertical distribution of potential temperature is shown in Fig. 91. Concerning the mechanism of this phenomenon, the following consideration seems reasonable to present writer.

* Manual of Meteorology. Vol. III. P. 27.

Although the pressure change is wave-like, it cannot be ascrided to the atmospheric waves. It is much more reasonable to regard it as a phase of convection. There is a surface current in the lower layer in the basin, when the cold north-westerly wind blows in the upper layer, the boundary between them being supposed to be 100–150m. high. The surface layer gets warmed by solar radiation during daytime, and rises in temperature along with the rise of the ground temperature. Even when the surface layer below has got warmed and is in a unstable state, it remains unbroken, up to a certain limit. Once that limit is reached, an overturn of the strata occurs. Then the upper cold

Fig. 90

(Microbarogram ; $\frac{1}{3}$ of original size)

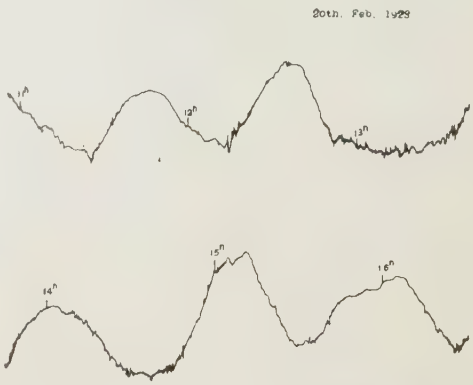

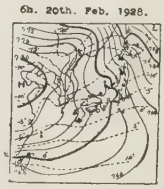

Fig. 92

Fig. 91

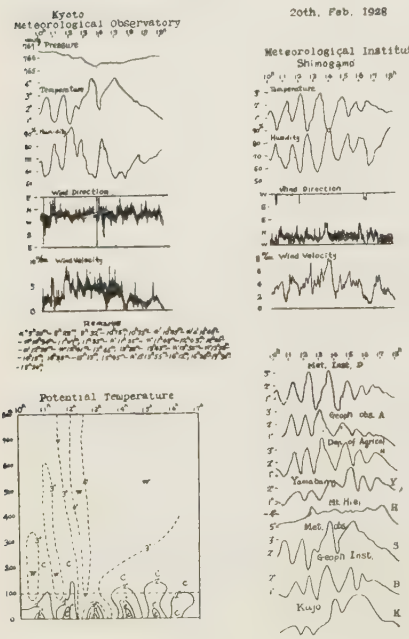

Fig. 93

(Microbarogram ; $\frac{1}{3}$ of original size)

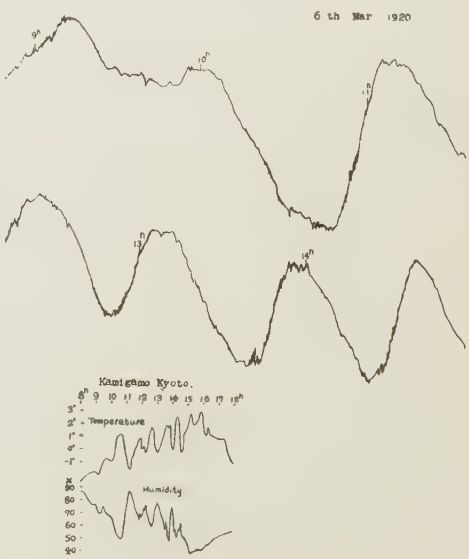

current descends to the surface of the earth, and the warm lower air rises. This is accompanied by an increase of wind velocity and pressure, a sudden fall of air temperature, and rain or snow. After the sudden commotion, everything returns to the former state of quiscence, and, once more, the surface layer begins to get warmed from below, the commencement of the repetition of this phenomenon. While the surface layer is getting warmed, the weather is fine, and a blue sky appears from time to time. The writer believes that, in this way, the records can be explained. What is noteworthy in this example is, that, though the periodic change of air temperature distinctly appears in the Kyôto Basin, it is not recorded on Mt. Hiei.

Another remarkable example occurring on the 6th Mar., 1920 is shown in Fig. 93. Similar phenomena, though not so striking as this, have been observed from time to time. Those recorded in 1928 are listed in Table 14.

Table 14

1928

Month	Day	Duration	No.	Remarkable Period	Weather	Wind Direction	Weather Type
Jan.	7	12^h-18^h	5	60min	S	NW	NW-ly
„	20	10—16	5	30	S	N	NW-ly
*Feb.	1	8—16	8	60	S	N-NW	NW-ly
* „	7	10—16	6	60	R	W-N	NW-ly
„	18	12—14	4	30	S	W-NW	NW-ly
„	20	10—16	6	30	S	W-NW	NW-ly
Mar.	11	10—16	7	60	S	W-NW	NW-ly
„	13	10—16	6	70		NW-N	NW-ly
„	14	12—16	4	60		NW-NNW	NW-ly
Apr.	7	8—16	6	70	R	NE-N	Anticyclone
„	23	10—15	5	40	R	W-NW	NW-ly
*Oct.	31	8—16	8	50	R	N-NE	NW-ly
Nov.	3	10—16	3	120	R	W-N	NW-ly
* „	10	8—14	8	40	R	N	NW-ly
* „	12	10—14	6	40	R	NW-NNE	NW-ly
„	17	10—17	5	70	R	NNE-NW	NW-ly
„	30	10—14	4	50	R	N-NW	NW-ly
*Dec.	10	9—14	6	40	R	N	NW-ly
„	25	10—14	5	40	R	N	NW-ly
„	29	10—14	3	120	R	N	NW-ly

S: Snow. R: Rain. * denotes a regular type.

3. Examples of Wave-like Pressure Changes with Longer Periods

In the first section of this Part, wave-like pressure changes with periods not longer than 20 min. are principally treated. Barometric oscillations much longer than these of course exist. Our instrument, however, being used for a different object, requires adjustment for waves with such long periods.* At any rate, it sometimes records striking pressure disturbances of great amplitude. These records may, on the whole, be regarded as true to the facts, and a few examples will be given below.

Fig. 94a, b, c, d

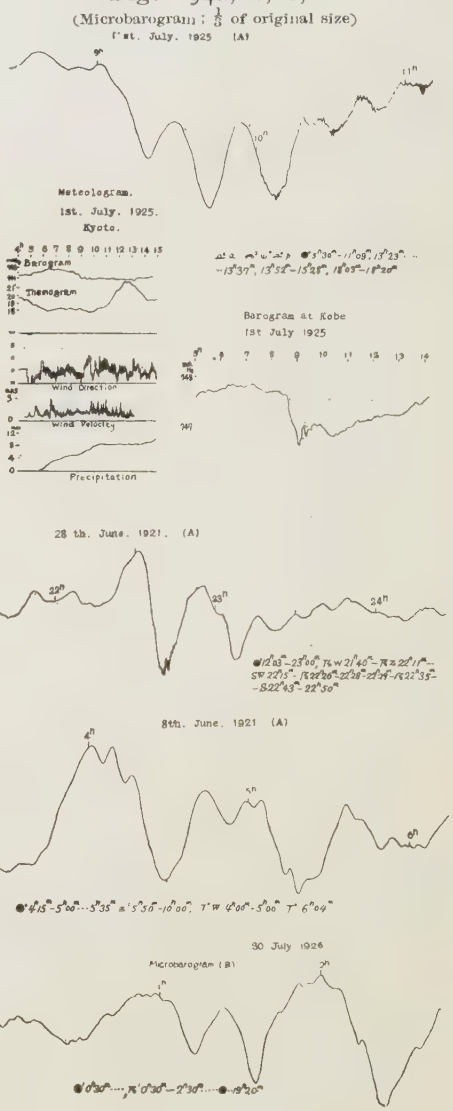

Ex. 1. 9–11 h, 1st July, 1925. (*Fig. 94a*) This accompanied a cyclonic trough. A very remarkable barometric oscillation with a period of about 25 min..

Ex. 2. 22–24 h, 28th June, 1921. (*Fig. 94b.*) *Ex. 3. 4–6 h, 8th June, 1921.* (*Fig. 94c.*) Both are pressure disturbances which occurred during night thunderstorms. They left on record a changing oscillation, with a period of about 25 min. in Ex. 2, and about 50 min. in Ex. 3.

Ex. 4. 1–3h, 30th June, 1926. (*Fig. 94d.*) This is, again, an instance of a pressure disturbance during a night thunderstorm. Its period and am-

* To be discussed in the last part.

plitude increase with the lapse of time. This increase has already been touched upon in the discussion of local showers.

All four of the above examples must have occurred in an upper layer, and all must have been pressure disturbances near an "Upper Front." The last example in particular must have been due to an overturn of the strata. Its mechanism is not yet clear to the writer, but, when fully investigated, it will be a great help to meteorologists who attempt to solve the structure of these disturbances.

4. Examples of Remarkable Pressure Disturbances Accompanied by a Sudden Change of Wind Vector

Ex. 1. 23 h 7th May, 1920. In Fig. 95 (a) the wind is fairly strong till about 22.5 h.. (Small rapid fluctuations on the record of the microbarograph indicate that there was a fairly strong wind.) Shortly after 22h, there is a sudden drop of wind, and the pressure disturbance occurs as shown in the figure, and accompanied by a thunderstorm. Along the boundary of two currents, striking pressure disturbances are often recorded, as this example shows.

Fig. 95 a, b

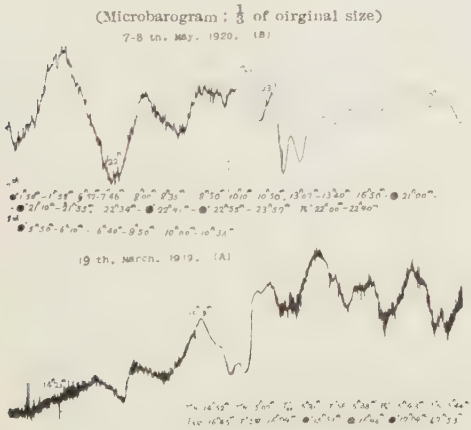

Ex. 2. 15 ½h, 19th March, 1919. In Fig. 95 (b) the speed of the wind suddenly decreases after 15h, a pressure disturbance occurring at the same time. This indicates that the centre of a secondary cyclone passed Kyôto, and that, in its centre, there was a small calm area, like the eye of a typhoon, with associated pressure disturbances. Thunder was heard at about 15h, but rain did not begin to fall till about 16 h.

Ex. 3. 6 h, 1st June, 1932. Fig. 96 (a) is a record taken at Kyôto. In this figure, at about 6½ h, the pressure rises about 3 mm. Hg. The wind presents no noteworthy feature at Kyôto; but on Mt. Hiei, a striking change in the character of the wind is observed, together with a pressure disturbance. (Fig. 96 b.) To be precise, while the pressure is maximum, the wind is neary calm, but it blows before and

after this disturbance at a speed of about 10 m/s. This remarkable change in the speed of the wind is observed likewise on Mt. Ibuki.

From these facts, is inferred that the sudden pressure rise is in some way related to the sudden change in the wind speed. This is one of the questions the present writer is trying to solve.

Fig. 96

(a) (b)

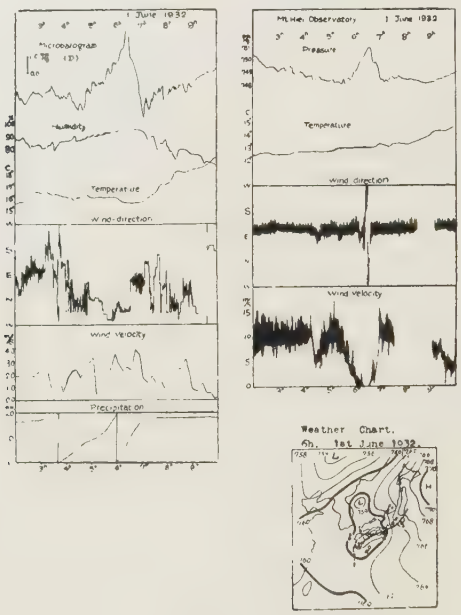

Fig. 97.

A Theory of Tunamis and Seiches produced by Wind and Barometric Gradient

By Takaharu Nomitsu

(Received June 12, 1935)

Abstract

This paper has been prepared from my previous papers on the "Coast effect upon the ocean current and sea level", in order to serve for investigations of the Tunamis caused by the typhoon that attacked the Kwansai District of Japan on Sept. 21 last year. At first, a correction is given to the ordinary formula for the steady value of surface elevation in shallow water, discarding the customary assumption that the elevation of surface is negligibly small compared with the total depth of the water. Next the development of tunamis and seiches under the condition of bottom-slip is dealt with in the case of varying causal action, and also extended to the case of progressive action. The viscosity of water, of course, is taken into account so that even for a perfectly resonancing action we can deduce reasonable results such as that the surface fluctuation cannot be amplified over $\pi/2$ times the steady value during half a period (or one crest) only of the causal force.

Introduction

On September 21 last year, a terrible typhoon attacked the Kwansai District and caused disastrous tunamis along the coasts of Ôsaka Bay and the Ki-i Channel, and also produced unprecedented undulations of water surface of Lake Biwa. The writer soon began to inspect and survey these tunami and seiche phenomena with his students and to collect mareo- and limnograms. In order to adjust the results thus obtained and explain them, an adequate theory of meteorological tunamis and seiches is highly desirable. Fortunately the writer's paper[1] on "Coast effect upon the ocean current and sea level" satisfies the demand with slight modifications, and may be taken as a theory of tunamis and seiches produced by wind and barometric gradient. The said paper will show that when a constant wind or barometric gradient begins to act upon a water basin and when after a time t it stops suddenly, then there occurs a rise of mean sea level generally accompanied by oscillations somewhat like those of Fig. 1, which are nothing but seiche oscillations; and if the level of the surface rises to such a degree that the water inundates the coast land, it may be

1. These Memoirs, **17**, 93–141 and 249–280 (1934)

called a tunami. Thus the meteorological tunamis and seiches are not essentially different in nature, and may be discussed together. Similarly we should expect the corresponding fluctuations of the water level whenever the motive forces increase or decrease *suddenly*.

The previous paper, however, was written from the view-point of ocean currents, and as a practical theory of tunamis and seiches

Fig. 1

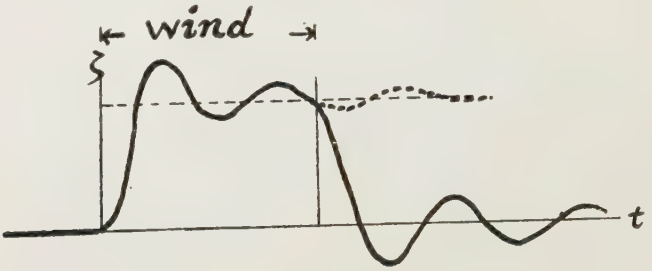

there remain several points to be modified or supplemented, while in some respects the theory may be simplified. For instance, in the theory of ocean currents the surface elevation may be considered negligibly small with respect to the depth of the sea, but, in the case of tunami it cannot be neglected, nay, it becomes rather greater than the usual depth of the shallow water near the coast. For the ocean current we may be content to consider the motive action as constant, but, when the problem of tunamis and seiches is under consideration, a varying or progressive force should be dealt with, resonance-effect playing an important part in the discussion.

On these problems, Dr. J. Proudman has written two papers. One[1] is very excellent as a theory of meteorological perturbations in a viscous canal with " no bottom-current ", but I believe that a rapid current in a shallow sea such as tunami must have considerable slip-velocity. Proudman's second paper[2] is also very original in dealing with the effect of progression and resonance due to the barometric change. Since the water there, however, is assumed as an ideal fluid (viscosity $\mu \equiv 0$), the method cannot be extended to the case of wind action, and even for the barometric action some[3] of the results will not necessarily coincide with that in the case $\mu \to 0$, especially when the barometric wave has a velocity $\sqrt{gH}$ resonancing with the water depth H.

1. Proc. London Math. Soc., **24**, 140 (1924)
2. Month. Not. Roy. Ast. Soc., Geophys. Suppl. **2**, 197 (1929)
3. Eq. (2. 3) and (2. 4) in his second paper.

The present paper has been prepared from my previous papers on the coast effect, and contains some improvements and supplements so as to cover the investigation of tunami due to wind and barometric change over a lake, a bay or a strait. In Chap. I, the steady value of surface elevation in shallow water is obtained without the ordinary assumption that the elevation is negligibly small compared with the total depth of the water. In Chap. II, the development of tunamis and seiches accompanied by the condition of bottom-slip, is dealt with in the case of varying causal action, and also extended to the case of progressive action. The viscosity of water is taken into account so that even for a perfectly resonancing action we can deduce reasonable results such as that the surface fluctuation cannot be amplified over $\pi/2$ times the steady value during half a period (or one crest) only of the causal force.

We shall here add that the rotation of the earth is neglected in this paper because the problem of meteorological tunami is, generally speaking, important only along the coast of a very shallow sea or in a long narrow bay.

I. Corrected formula for the steady value of the tunami produced by wind along a shallow-water coast

§ 1. Customary formula and the necessity for its correction. Both in the empirical formula of Colding[1] and in the theoretical formula of Ekman[2], the surface elevation ζ in a canal produced by wind may be expressed in the form

$$\frac{\Delta\zeta}{\Delta L}=\gamma=n\frac{T}{g\rho H} \quad \ldots\ldots(1)$$

where γ denotes the surface slope, H the depth of the sea, T the tangential stress of wind, g the acceleration of gravity, ρ the density of water respectively, and n is a coefficient which becomes $3/2$ with Ekman's assumption of no bottom-current.

According to the writer's paper[3] on the coast effect, the coefficient will take the value $n=1$ for no bottom-friction. In the case of finite bottom-friction, putting $\omega=0$ in the said paper, we shall get

$$n=\frac{1+f'\rho H/2\mu}{1+f'\rho H/3\mu} \qquad \text{if bottom-friction}=f'\rho u_H, \quad \ldots\ldots\ldots(2)$$

and

$$n=\frac{3}{2}\left\{1+\frac{3\mu^2}{f\rho H^2 T}\left(1-\sqrt{1+\frac{2}{9}\frac{f\rho H^2 T}{\mu^2}}\right)\right\} \quad \ldots\ldots\ldots(2')$$

1. Kgl. Danske Vidensk. Selsk. Skrifter, **1**, 272 (1880).
2. Ark. f. Mat. Ast. o. Fys. **2**, No. 11 (1905). 3. op. cit.

if bottom-resistance $=f\rho u_H^2$, where u_H denotes the slip-velocity at the bottom. All the above formulae, however, were derived on the supposition that the level rise ζ is negligibly small compared with the depth of the sea, and hence they are obviously not applicable, as they stand, to the investigation of tunamis so high as to invade the land. For instance, if the sea bottom make an inclined plane, formula (1) will give infinite γ and consequently infinite elevation of water at the coast ($H=0$). To avoid this impropriety, as some investigators have done, if we divide the sea into several portions for each of which formula (1) is applied with respective mean depth, and if we take the sum of the elementary rises of level $\Delta\zeta$ thus obtained as the height of tunami ζ at the coast, then we shall get a finite rise, but the value will be indeterminate according to the degree of division of the sea. Really the last landward portion of the sea of inclined plane bottom, however narrow may be taken, will give an identical value

$$\Delta\zeta=n\frac{T\cdot\Delta L}{g\rho\cdot H/2}=n\frac{2T}{g\rho\cdot\tan\theta}\qquad(\theta=\text{Angle of inclination of the bottom}),$$

which is independent of the length of that portion of the sea. Thus, for the purpose of rough estimation of the order of tunami we may simply put the mean depth of the whole basin for H in formula (1), but in order to discuss more precisely the tunami problem at the coast we should first attempt to improve the formula, without disregarding the level rise ζ in comparison with H.

It may here be added that the steady value of the surface elevation due to the barometric gradient will not differ from the statical value even for very shallow water.

§ 2. **Corrected formula for a sea of no bottom-current.** If, after Ekman, we assume no bottom-current the motion of water in a one-directional canal in a steady state will be expressed in the ordinary notations, as follows:

$$\mu\frac{\partial^2 u}{\partial z^2}-g\rho\frac{d\zeta}{dx}=0 \qquad \ldots\ldots(3)$$

with the conditions

$$-\mu\partial u/\partial z=T \text{ at the surface } (z=-\zeta) \qquad \ldots(4)$$

$$u=0 \text{ at the bottom } (z=H) \qquad \ldots(5)$$

and

$$S\equiv\int_{-\zeta}^{H}u\,dz=0 \qquad \ldots\ldots(6)$$

where positive z is taken downward from the undisturbed water-surface and the disturbed surface is put as $z=-\zeta$.

Now the first integral of (3) is

$$\mu\frac{\partial u}{\partial z}=g\rho\frac{d\zeta}{dx}z+A \qquad \ldots\ldots(7)$$

which combined with (4) gives

$$T=g\rho\frac{d\zeta}{dx}\zeta-A. \qquad \ldots\ldots(8)$$

The second integral is $$\mu u=\frac{g\rho}{2}\frac{d\zeta}{dx}z^2+Az+B \quad \ldots\ldots(9)$$

which becomes by the condition (5)

$$\mu u=\frac{g\rho}{2}\frac{d\zeta}{dx}(z^2-H^2)+A(z-H). \quad \ldots\ldots\ldots(9')$$

Then the equation of continuity (6) will give

$$0=g\rho\frac{d\zeta}{dx}\frac{2H^3+3H^2\zeta-\zeta^3}{3(H+\zeta)^2}+A. \quad \ldots\ldots\ldots\ldots(10)$$

Eliminating A from (8) and (10), we get $$\frac{d\zeta}{dx}=\frac{3}{2}\frac{T}{g\rho(H+\zeta)}. \quad (11)$$

This is the corrected formula for the surface slope due to the wind and shows that precisely we must use the actual depth $H+\zeta$ instead of H in eq. (1).

§ **3. Case of bottom-slip.** If some slip-velocity u_H exists at the bottom and the bottom condition is replaced by

$$-|\mu\ \partial u/\partial z|_{H=z}=f'\rho u_H \quad \ldots\ldots\ldots\ldots\ldots\ldots(5')$$

instead of (5), then the first integral (7) will give

$$T=g\rho\frac{d\zeta}{dx}\cdot\zeta-A \quad \ldots(8), \qquad -f'\rho u_H=g\rho\frac{d\zeta}{dx}H+A. \quad \ldots(12)$$

The bottom-current u_H is also obtained from the second integral (9)

$$\mu u_H=\frac{g\rho}{2}\frac{d\zeta}{dx}H^2+AH+B \quad \ldots\ldots\ldots\ldots\ldots(13)$$

Eq. of continuity (6) will give by substitution of (9)

$$\frac{g\rho}{2}\frac{d\zeta}{dx}\frac{H^2-H\zeta+\zeta^2}{3}+A\frac{H-\zeta}{2}+B=0\ldots\ldots(14)$$

The above four equations (8), (12), (13) and (14) serve to determine four unknowns A, B, u_H, $\frac{d\zeta}{dx}=\gamma$. Specially, if there is no bottom-friction and $f'=0$, the surface slope can be obtained from (8) and (12) only, namely $$\gamma=\frac{d\zeta}{dx}=\frac{T}{g\rho(H+\zeta)}. \quad \ldots\ldots(11_a)$$

When $f'\neq 0$ generally, however, we proceed as follows:—

From (8) and (12) $$-f'\rho u_H=g\rho\gamma(H+\zeta)-T,$$

and from (8) and (13) $$\mu u_H=g\rho\gamma H\left(\frac{H}{2}+\zeta\right)-TH+B.$$

Therefore $$0=g\rho\gamma\left[\frac{\mu}{f'\rho}(H+\zeta)+H\left(\frac{H}{2}+\zeta\right)\right]-T\left(\frac{\mu}{f'\rho}+H\right)+B.$$

Combining this with the following relation

$$\frac{g\rho}{2}\gamma\left[\frac{H^2-H\zeta+\zeta^2}{3}+(H-\zeta)\zeta\right]-\frac{T}{2}(H-\zeta)+B=0$$

obtained from (8) and (14), we have

$$\gamma=\frac{d\zeta}{dx}=n\frac{T}{g\rho(H+\zeta)} \qquad \text{.....(15)}$$

where $$n=\left(1+\frac{f'\rho(H+\zeta)}{2\mu}\right)\Big/\left(1+\frac{f'\rho(H+\zeta)}{3\mu}\right). \qquad \text{.....(16)}$$

Thus we see that the more precise formula for the surface slope is obtained by putting $H+\zeta$ instead of all H's in the formula given in § 1. The same may be also said when the bottom-friction is equal to $f\rho u_H^2$.

It is here to be noticed that the coefficient n will reduce to 1 if $f'=0$ (no bottom-friction) and to $3/2$ if $f'=\infty$ (no bottom-current), and that, with finite values of f' and μ, the value of n for a very shallow sea ($H\fallingdotseq 0$) tends to that for "no bottom-friction" and a very deep sea resembles that of "no bottom-current". Morever, since ζ in the expression of n in (16) enters in both numerator and denominator in a similar manner, its effect will be comparatively slight so that we may omit it for practical purposes, while ζ in (15) may occasionally have great importance.

§ 4. **Evaluation of surface elevation ζ.** In order to evaluate the rise of water at the coast we must know the functional relation of H and x. If the relation $H=f(x)$ is complicated, we divide the sea into many portions and calculate $\zeta=\Sigma\Delta\zeta=\Sigma n\frac{T}{g\rho(H+\zeta)}\Delta x$. .....(17)

Of course, we begin with those portions in which ζ is negligible compared with H, and when we reach a portion such that the sum of the preceeding $\Delta\zeta$ becomes comparable with H, obtain $H+\zeta$ for the end of that portion and, by using it, calculate $\Delta\zeta$ and hence the next ζ, and so on. When $H=f(x)$ is a simple function, the direct integration of (16) in a finite form is much more convenient. The following two cases are very important in practice.

(Ex. 1) *Uniform shallow water.* If $H=$constant, taking the origin of x at the place of $\zeta=0$, we have $\zeta=H\left\{\sqrt{1+2n\frac{T}{g\rho H^2}x}-1\right\}$.

(Ex. 2) *Sea of inclined plane bottom.* If the shallow sea has a plane bottom inclined at an angle θ with the horizontal, take the origin of x at the end of the plane bottom where the depth is H_0 and the

distance from the coast is L. Then at any x landwards, the depth of the undisturbed sea will be (Fig. 2)

$$H=H_0-x\tan\theta=H_0(1-x/L) \qquad \text{.....(18)}$$

Fig. 2

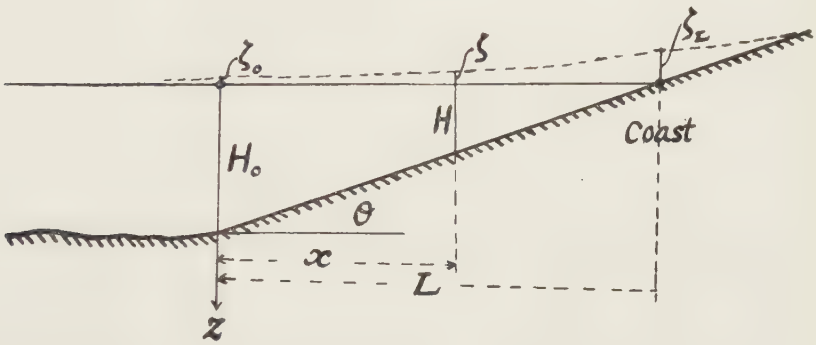

and the integral of (15) will become

$$\zeta+\bar{\xi}_{H_0}\log\{1-(H_0+\zeta-x\tan\theta)/\bar{\xi}_{H_0}\}=C \qquad \text{.....(19)}$$

where $$\bar{\xi}_{H_0}=n\frac{T}{g\rho H_0}L=n\frac{T}{g\rho\tan\theta} \qquad \text{.....(20)}$$

and C is the integration constant. In order to determine the constant C, the constancy of water in the whole sea, i. e., $\int\zeta dx=0$ .....(21) will serve generally. For actual seas we can often easily estimate

$\zeta=\zeta_0$ at $x=0$ ...(21′) so that the constant C can be determined. For instance, a lake with a symmetrical profile will have no ζ at the center, and even for a common sea, the elevation up to the place of depth H_0 (usually moderate depth) may be calculated by the approximate formula (1) starting from the open deep part.

In such cases, eq. (19) may be written

$$\zeta=\zeta_0+\bar{\xi}_{H_0}\log\frac{\bar{\xi}_{H_0}-(H_0+\zeta_0)}{\bar{\xi}_{H_0}-(H_0+\zeta-x\tan\theta)}. \qquad \text{.....(19′)}$$

Let ζ_L represent the elevation at the coast line ($x=L$), then it will be given by $$\zeta_L=\zeta_0+\bar{\xi}_{H_0}\log\frac{H_0+\zeta_0-\bar{\xi}_{H_0}}{\zeta_L-\bar{\xi}_{H_0}} \qquad \text{.....(22)}$$

Specially, if ζ_0 is 0 or negligibly small,

$$\zeta_L/\bar{\xi}_{H_0}+\log(\zeta_L/\bar{\xi}_{H_0}-1)=\log(H_0/\bar{\xi}_{H_0}-1) \qquad \text{.....(22′)}$$

where $\bar{\xi}_{H_0}=n\,TL/g\rho H_0$ denotes the rise of wat r at the coast, supposing the sea to be of uniform depth H_0, and $2\bar{\xi}_{H_0}$ corresponds to that given by eq. (1) for the actual sea under consideration.

Table 1 is prepared for practical convenience, by calculating inversely the corresponding values of H_0 for given values of ζ_L.

Table 1. Relation between ζ_L and H_0 when $\zeta_0 \fallingdotseq 0$

$\zeta_L/2\xi_{H_0}$	0	0.25	0.5	0.75	1.0	1.5	2.0	2.5	5
ζ_L/ξ_{H_0}	0	0.5	1	1.5	2.0	3.0	4.0	5.0	10
H_0/ξ_{H_0}	0	0.09	1	3.24	8.39	41.2	165	595	198400

II. Changing state in a canal with finite bottom-friction

§ 5. Constant motive action over a lake or an enclosed sea.

The changing state dealt with in my previous paper on the coast effect, II, corresponds to the steady value (1) in this paper, namely it stands on the assumption that $\zeta \ll H$, and therefore it might seem necessary to re-investigate the problem carefully, taking the water surface as $z=-\zeta$ but not $z=0$. From the practical viewpoint, however, this will be unnecessary. For, although the final values of the exact solution may be very different from those of approximate solution as explained in Chapter I, the mode of development will not differ greatly. Thus it will be practically sufficient to assume that, even in the accurate solution, the functional relation to the time is nearly the same as before except that the steady value contained in the coefficient must be replaced by the corrected formula given in the preceeding chapter.

Now, for the two extreme cases of " no bottom-current " and " no bottom-friction " the development of surface elevation was discussed in sufficient detail in the previous papers. For " finite bottom-friction ", however, it was only shown that the development can be investigated in an entirely similar manner, the actual calculation in a definite formula being omitted. However, since the last case is obviously most probable in reality, we shall here make definite the formal solution given in the previous paper for level rise in a uniform canal with finite bottom-friction, as a preparation for the investigation of actual tunamis and seiches caused by the recent violent typhoon.

Consider a constant wind T or a barometric gradient γ_0 (measured in water column) begin to act suddenly all over the water initially at rest, and let a surface slope $\gamma=-\partial\zeta/\partial x$ be generated. Then the equation of motion will be represented by

$$\left.\begin{aligned} \frac{\partial u}{\partial t} &= \nu\frac{\partial^2 u}{\partial z^2}+g\gamma \qquad \text{for wind,} \qquad \nu=\mu/\rho, \\ &= \nu\frac{\partial^2 u}{\partial z^2}+g(\gamma+\gamma_0) \quad \text{for barometric gradient,} \end{aligned}\right\} \ldots(23)$$

with the conditions

at surface ($z=0$), $-\mu\partial u/\partial z = T$ for wind action; $=0$ for barom. grad., ...(24)

at bottom ($z=H$), $-\mu\partial u/\partial z = f'\rho u_H$, ...(25)

initially ($t=0$) $u=\gamma=0$, ...(26)

and eq. of continuity

$$\frac{\partial\zeta}{\partial t} = -\frac{\partial S}{\partial x} \quad \text{or} \quad \frac{\partial\gamma}{\partial t} = \frac{\partial^2 S}{\partial x^2}, \qquad \text{where} \quad S=\int_0^H u dz. \qquad \text{.....(27)}$$

Such u which satisfies eqs. (23) to (26) can be easily obtained by taking the limit when $\omega=0$ in our previous paper, or by solving independently though in a manner entirely analogous to that there used; and in any case we shall get

$$u = F\sum A_n \cos\beta_n z\,(1-e^{-\nu\beta_n^2 t}) + \sum B_n \cos\beta_n z \int_0^t \gamma(\tau) e^{-\nu\beta_n^2(t-\tau)} d\tau \quad \text{...(28)}$$

where $\beta_n \tan\beta_n H = f'\rho/\mu \equiv h$ (say), ...(29)

$F=T$ for wind action; $=\gamma_0$ for barometric gradient, ...(30)

$$A_n = \frac{2(\beta_n^2+h^2)}{H(\beta_n^2+h^2)+h}\cdot\frac{1}{\mu\beta_n^2} \quad \text{for wind}$$
$$= \frac{2(\beta_n^2+h^2)}{H(\beta_n^2+h^2)+h}\cdot\frac{g\sin\beta_n H}{\nu\beta_n^3} \quad \text{for barom. grad.,} \qquad \text{...(31)}$$

and $$B_n = g\cdot\frac{2(\beta_n^2+h^2)}{H(\beta_n^2+h^2)+h}\cdot\frac{\sin\beta_n H}{\beta_n}. \qquad \text{.....(32)}$$

These may also be directly verified by substitution in eqs. (23) to (26), and A_n corresponds to the coefficients when the steady value[1] of pure drift or barometric current is expanded in such a series as $F\sum A_n\cos\beta_n z$. Now, the total flow S becomes

$$S=\int_0^H u dz = F\sum A_n \frac{\sin\beta_n H}{\beta_n}(1-e^{-\nu\beta_n^2 t}) + \sum B_n \frac{\sin\beta_n H}{\beta_n}\int_0^t \gamma(\tau) e^{-\nu\beta_n^2(t-\tau)} d\tau, \qquad \text{.....(33)}$$

of which, for the reasons mentioned in the previous paper, only terms with $n=0$ may be introduced in eq. of continuity (27). Then we get

---

1. Steady drift current $= \frac{T}{f'\rho} + \frac{T}{\mu}(H-z)$,

Steady barom. current $= g\rho\gamma_0\left(\frac{H}{f'\rho} + \frac{H^2-z^2}{2\mu}\right)$.

$$\frac{\partial\gamma}{\partial t}=\frac{d^2F}{dx^2}\frac{A_0\sin\beta_0H}{\beta_0}(1-e^{-\nu\beta_0^2t})$$
$$+B_0\frac{\sin\beta_0H}{\beta_0}\int_0^t\frac{\partial^2\gamma(\tau)}{\partial x^2}e^{-\nu\beta_0^2(t-\tau)}d\tau, \quad \cdots\cdots(34)$$

which, combined with its second time-derivative, gives

$$\frac{\partial^2\gamma}{\partial t^2}+\nu\beta_0^2\frac{\partial\gamma}{\partial t}-B_0\frac{\sin\beta_0H}{\beta_0}\frac{\partial^2\gamma}{\partial x^2}=\frac{d^2F}{dx^2}\frac{A_0\sin\beta_0H}{\beta_0}\cdot\nu\beta_0^2. \quad \cdots(35)$$

If the canal is of length L, and if we put

$$\left.\begin{aligned}&\gamma=\sum\gamma_m\sin\frac{m\pi}{L}x, \quad \frac{\partial^2\gamma}{\partial x^2}=\sum\gamma_m''\sin\frac{m\pi}{L}x, \quad \gamma_m''=-\left(\frac{m\pi}{L}\right)^2\gamma_m,\\ &F=\sum F_m\sin\frac{m\pi}{L}x, \quad \frac{\partial^2F}{\partial x^2}=\sum F_m''\sin\frac{m\pi}{L}x, \quad F_m''=-\left(\frac{m\pi}{L}\right)^2F_m,\end{aligned}\right\}(36)$$

then (35) will give

$$\frac{d^2\gamma_m}{dt^2}+\nu\beta_0^2\frac{d\gamma_m}{dt}+B_0\frac{\sin\beta_0H}{\beta_0}\left(\frac{m\pi}{L}\right)^2\gamma_m=-A_0\nu\beta_0\sin\beta_0H\cdot\left(\frac{m\pi}{L}\right)^2F_m,$$
$$\cdots\cdots(37)$$

whose solution is evidently

$$\left.\begin{aligned}\gamma_m(t)&=\bar\gamma_m\left[1-e^{-\frac{1}{2}\nu\beta_0^2t}\left\{\cos\sigma_mt+\frac{\nu\beta_0^2}{2\sigma_m}\cdot\sin\sigma_mt\right\}\right]\\ &=\bar\gamma_m\left[1-\frac{\sqrt{4\sigma_m^2+(\nu\beta_0^2)^2}}{2\sigma_m}e^{-\frac{1}{2}\nu\beta_0^2t}\cos(\sigma_mt-\varepsilon)\right],\end{aligned}\right\}\cdots(38)$$

where

$$\left.\begin{aligned}&\sigma_m=\sqrt{B_0\frac{\sin\beta_0H}{\beta_0}\left(\frac{m\pi}{L}\right)^2-\left(\frac{\nu\beta_0^2}{2}\right)^2},\\ &\tan\varepsilon=\nu\beta_0^2/2\sigma_m, \quad \text{damping factor}=e^{-\frac{1}{2}\nu\beta_0^2t},\end{aligned}\right\}\cdots\cdots(39)$$

and $\bar\gamma_m$, though equal to $-\nu\beta_0^2F_m\cdot A_0/B_0$ in mathematical expression, is physically the final value of $\gamma_m(t)$, so that it may be taken as the element in Fourier's series for the already known steady value of slope

$$\left.\begin{aligned}\bar\gamma&=nT/g\rho H \quad &&\text{for wind action}\\ &=\gamma_0 &&\text{for barometric action.}\end{aligned}\right\}\cdots\cdots(40)$$

Eq. (39) shows also that the development of the slope will be oscillatory or non-oscillatory, according as

$$\frac{4B_0\sin\beta_0H}{\nu^2\beta_0^5}\left(\frac{m\pi}{L}\right)^2>1 \text{ or } <1.$$

Finally it is to be noticed that the above solution has the same form as that found in the case of "no bottom-current" and described in the previous paper, i. e., the mode of development of the phenomena will be entirely similar, the only difference being in the final value $\bar\gamma_m$ according to the condition of bottom and the kind of motive force (wind or barometric).

§ 6. **Variable action.** If the motive force F is variable with the time, $\bar{\gamma}_m$ proportional to F_m varies also with time such that $\bar{\gamma}_m = \bar{\gamma}_m(t)$. Then, applying the writer's newly established theorem to eq. (38), we easily get

$$\gamma_m(t) = \int_0^t \frac{\partial \bar{\gamma}_m(\tau)}{\partial \tau} \left\{ 1 - \frac{\sqrt{4\sigma_m^2 + (\nu\beta_0^2)^2}}{2\sigma_m} \cos\{\sigma_m(t-\tau) - \varepsilon\} e^{-\frac{1}{2}\nu\beta_0^2(t-\tau)} \right\} d\tau. \quad \cdots\cdots\cdots\cdots\cdots\cdots (41)$$

Similarly the elementary surface-elevation ζ_m corresponding to γ_m will be given by

$$\left.\begin{aligned} \zeta_m(t) &= \int_0^t \frac{\partial \bar{\xi}_m(\tau)}{\partial \tau} \left\{ 1 - \frac{\sqrt{4\sigma_m^2 + (\nu\beta_0^2)^2}}{2\sigma_m} \cos\{\sigma_m(t-\tau) - \varepsilon\} e^{-\frac{1}{2}\nu\beta_0^2(t-\tau)} \right\} d\tau \\ &= \bar{\xi}_m(t) - \frac{\sqrt{4\sigma_m^2 + (\nu\beta_0^2)^2}}{2\sigma_m} \int_0^t \frac{\partial \bar{\xi}_m(\tau)}{\partial \tau} \cos\{\sigma_m(t-\tau) - \varepsilon\} e^{-\frac{1}{2}\nu\beta_0^2(t-\tau)} d\tau, \end{aligned}\right\} (42)$$

where $\bar{\xi}_m$ is the steady value of surface elevation corresponding to $\bar{\gamma}_m$.

Since the level change expressed by (42) is generally of ocillatory nature, which is nothing but seiche motion, and since it may become tunami if the rise attains an exceptional height, we may take eq. (42) as representing *a general theory of meteorological tunamis and seiches.*

If the motive force F is a simple function of time, the above formula may of course be integrated in finite form, as seen at the end of my paper on the drift current in the ocean, I. However complicated the variation of the motive force with the time may be, the mechanical quadrature of eq. (42) will enable us to determine the change of surface level from time to time. The writer has made actual evaluations for the tunami at Ôsaka and the abnormal fluctuation of level of Lake Biwa caused by the recent typhoon, and the results will be described in subsequent papers. Moreover, eqs. (29), (39) and (40) will serve to estimate three unknowns f', ν and β_0, by measuring the amplitudes and periods of fluctuation from the actual mareo- or limnograms. Specially if $f' =$ very small, (29) becomes $\nu\beta_0^2 = f'/H$; and f' can be determined by the measurement of the damping factor only.

§ 7. **Resonance effect.** Eq. (42) includes of course the resonance effect when the motive force varies with a period nearly equal to the proper period of the sea. For example, let us consider here a simple case in which the motive force, and consequently $\bar{\xi}_m$, is a sine function of time, i. e.,

$$\left.\begin{aligned} \bar{\xi}_m &= Z\sin(\sigma' t + \alpha) \quad \text{for } 0 \leqq t \leqq t_1, \\ &= 0 \quad \text{for } t < 0 \text{ and } t > t_1. \end{aligned}\right\} \quad \cdots\cdots\cdots\cdots (43)$$

Then eq. (42) gives: For $t < t_1$ (during the action of the motive force),

$$\zeta_m(t)=Z.\frac{\sigma_m^2+\left(\frac{1}{2}\nu\beta_0^2\right)^2}{2\sigma_m}\times$$

$$\left[\frac{1}{\left(\frac{1}{2}\nu\beta_0^2\right)^2+(\sigma_m+\sigma')^2}\left\{\begin{array}{l}\frac{1}{2}\nu\beta_0^2\cos(\sigma' t+\alpha)+(\sigma_m+\sigma')\sin(\sigma' t+\alpha)\\ -e^{-\frac{1}{2}\nu\beta_0^2 t}\left[\frac{1}{2}\nu\beta_0^2\cos(\sigma_m t-\alpha)\right.\\ \qquad\left.-(\sigma_m+\sigma')\sin(\sigma_m t-\alpha)\right]\end{array}\right\}\right.$$

$$\left.-\frac{1}{\left(\frac{1}{2}\nu\beta_0^2\right)^2+(\sigma_m-\sigma')^2}\left\{\begin{array}{l}\frac{1}{2}\nu\beta_0^2\cos(\sigma' t+\alpha)-(\sigma_m-\sigma')\sin(\sigma' t+\alpha)\\ -e^{-\frac{1}{2}\nu\beta_0^2 t}\left[\frac{1}{2}\nu\beta_0^2\cos(\sigma_m t+\alpha)\right.\\ \qquad\left.-(\sigma_m-\sigma')\sin(\sigma_m t+\alpha)\right]\end{array}\right\}\right] \quad (44a)$$

For $t>t_1$ (after the motive force has ceased to act), since

$$\int_0^t\bar{\xi}_m(\tau)\phi(t-\tau)d\tau=\int_0^{t_1}\bar{\xi}_m(\tau)\phi(t-\tau)d\tau+\int_{t_1}^t 0\times\phi(t-\tau)d\tau$$

$$=\int_0^{t_1}\bar{\xi}_m(\tau)\phi(t-\tau)d\tau,$$

$$\zeta_m(t)=Z.\frac{\sigma_m^2+\left(\frac{1}{2}\nu\beta_0^2\right)^2}{2\sigma_m}\times$$

$$\left[\frac{1}{\left(\frac{1}{2}\nu\beta_0^2\right)^2+(\sigma_m+\sigma')^2}\left\{\begin{array}{l}e^{-\frac{1}{2}\nu\beta_0^2(t-t_1)}\left[\frac{1}{2}\nu\beta_0^2\cos\{\sigma_m t-(\sigma_m+\sigma')t_1-\alpha\}\right.\right.\\ \qquad\left.-(\sigma_m+\sigma')\sin\{\sigma_m t-(\sigma_m+\sigma')t_1-\alpha\}\right]\\ -e^{-\frac{1}{2}\nu\beta_0^2 t}\left[\frac{1}{2}\nu\beta_0^2\cos(\sigma_m t-\alpha)\right.\\ \qquad\left.-(\sigma_m+\sigma')\sin(\sigma_m t-\alpha)\right]\end{array}\right\}\right.$$

$$\left.-\frac{1}{\left(\frac{1}{2}\nu\beta_0^2\right)^2+(\sigma_m-\sigma')^2}\left\{\begin{array}{l}e^{-\frac{1}{2}\nu\beta_0^2(t-t_1)}\left[\frac{1}{2}\nu\beta_0^2\cos\{\sigma_m t-(\sigma_m-\sigma')t_1+\alpha\}\right.\right.\\ \qquad\left.-(\sigma_m-\sigma')\sin\{\sigma_m t-(\sigma_m-\sigma')t_1+\alpha\}\right]\\ -e^{-\frac{1}{2}\nu\beta_0^2 t}\left[\frac{1}{2}\nu\beta_0^2\cos(\sigma_m t+\alpha)\right.\\ \qquad\left.-(\sigma_m-\sigma')\sin(\sigma_m t+\alpha)\right]\end{array}\right\}\right] \quad \ldots\ldots\ldots\ldots\ldots\ldots\ldots\ldots(44b)$$

If $\nu\to 0$ and $t<t_1$, (44a) gives

$$\zeta_m=\frac{Z}{2}\left[\frac{\sigma_m}{\sigma_m+\sigma'}\{\sin(\sigma' t+\alpha)+\sin(\sigma_m t-\alpha)\}\right.$$

$$\left.+\frac{\sigma_m}{\sigma_m-\sigma'}\left\{\sin(\sigma' t+\alpha)-\sin(\sigma_m t+\alpha)\right\}\right] \quad \ldots\ldots(44'a)$$

which, when $\sigma' \to \sigma_m$, becomes

$$\zeta_m = \frac{Z}{2}\{\cos\alpha \sin\sigma' t - \sigma' t \cos(\sigma' t + \alpha)\}. \quad \ldots\ldots\ldots\ldots(45a)$$

For $\infty > t > t_1$, the corresponding formula will be

$$\zeta_m = \frac{Z}{2}\left[\sin\sigma' t_1 \cos\{\sigma'(t-t_1)-\alpha\} - \sigma' t_1 \cos(\sigma' t + \alpha)\right]. \quad \ldots\ldots\ldots\ldots(45b)$$

Thus, if t_1 is large, the amplitude will increase greatly with time; but when t_1 is small, the amplitude will not be so much enlarged even for a period of perfect resonance. For example, if t_1 = half a period i. e. $\sigma' t_1 = \pi$ (only one crest of force), the maximum value of ζ_m cannot exceed $\frac{1}{2}\pi Z$, and when t_1 = a complete period, the possible maximum value is $\zeta_m = \pi Z$.

§ 8. **Seiches and tunamis in a bay, a shelf sea or a strait.** All the above investigations have been restricted to an enclosed sea or a lake of length L, but they can very easily be extended to a bay, a continental shelf sea and a strait. For a bay, it is unnecessary to say that the phenomena will be the same as for a symmetrical lake half of which coincides with the given bay. The so-called continental shelf sea, whose depth diminishes sharply from the continuing ocean depth, will act like a bay in this respect, because both seas are equally characterised by an abrupt contraction of cross-section at the entrance, where level fluctuation must have a node. Thus the seiches and tunamis of meteorological origin in a bay or a continental shelf sea can be discussed by the foregoing formula, in which L must be taken as twice the length of the bay or the shelf sea.

Lastly for a strait of length L, we expand the motive force F and consequently $\bar{\gamma}$ and $\bar{\xi}$ in forms

$$F = \sum F_m \cos\frac{m\pi}{L}x, \quad \bar{\gamma} = \sum \bar{\gamma}_m \cos\frac{m\pi}{L}x, \quad \bar{\xi} = \sum \bar{\xi}_m \sin\frac{m\pi}{L}x, \quad (36')$$

instead of (36). Then exactly the same equations as (38) to (45) are obtained.

§ 9. **Progressive motive force in an endless canal.** In order to estimate the effect of advance of a motive force, let us consider the case in which

$$\left.\begin{array}{ll} \bar{\zeta} = Z\sin(\sigma' t - lx) & 0 \leqq t \leqq t_1 \\ \quad = 0 & t < 0 \text{ and } t > t_1, \end{array}\right\} \quad \ldots\ldots\ldots(46)$$

with initial condition $\zeta = u = 0$ for $t \leqq 0$.

Since $\bar{\zeta} = Z[\sin\sigma' t \cos lx + \sin(\sigma' t - \pi/2)\sin lx]$,

ζ_m = that in a bay (with $\alpha = 0$) + that in a strait (with $\alpha = -\pi/2$)
= {cos $lx \times$ eq. (44) with $\alpha = 0$} + {sin$lx \times$ eq. (44) with $\alpha = -\pi/2$}.

i. e.
$$\zeta_m = Z \frac{\sigma_m^2 + \left(\frac{1}{2}\nu\beta_0^2\right)^2}{2\sigma_m} \left[\frac{1}{\left(\frac{1}{2}\nu\beta_0^2\right)^2 + (\sigma_m + \sigma')^2} \times \left\{ \begin{array}{l} \frac{1}{2}\nu\beta_0^2 \cos(\sigma' t - lx) + (\sigma_m + \sigma')\sin(\sigma' t - lx) \\ - e^{-\frac{1}{2}\nu\beta_0^2 t}\left[\frac{1}{2}\nu\beta_0^2 \cos(\sigma_m t + lx) - (\sigma_m + \sigma')\sin(\sigma_m t + lx) \right] \end{array} \right\} \right.$$
$$\left. - \frac{1}{\left(\frac{1}{2}\nu\beta_0^2\right)^2 + (\sigma_m - \sigma')^2} \left\{ \begin{array}{l} \frac{1}{2}\nu\beta_0^2 \cos(\sigma' t - lx) \\ \quad - (\sigma_m - \sigma')\sin(\sigma' t - lx) \\ \quad - e^{-\frac{1}{2}\nu\beta_0^2 t}\left[\frac{1}{2}\nu\beta_0^2 \cos(\sigma_m t - lx) \right. \\ \quad \left. - (\sigma_m - \sigma')\sin(\sigma_m t - lx) \right] \end{array} \right\} \right] \qquad (47a)$$

for $t < t_1$. Specially if $\nu \to 0$, the above eq. becomes

$$\zeta_m = \frac{Z}{2}\left[\frac{1}{1 + \sigma'/\sigma_m}\{\sin(\sigma' t - lx) + \sin(\sigma_m t + lx)\} + \frac{1}{1 - \sigma'/\sigma_m}\{\sin(\sigma' t - lx) - \sin(\sigma_m t - lx)\} \right], \quad \ldots\ldots\ldots (47'a)$$

Farther when $\sigma' \to \sigma_m$,

$$\zeta_m \doteqdot \frac{Z}{2}\left[\cos lx \sin\sigma' t - \sigma' t \cos(\sigma' t - lx) \right]. \quad \ldots\ldots\ldots (47''a)$$

For $\infty > t > t_1$, also, a similar procedure can be used.

Here we notice that all these equations in the present paragraph will be obtained by putting $-lx$ instead of α in eqs. (44) and (45); and eq. (47″a) shows that the resonance effect will be such as explained in the preceding article. Eq. (47′a) coincides with that given by Proudman, (2.4), and is valid only when $\sigma_m \backsim \sigma' \gg \frac{1}{2}\nu\beta_0^2$ and $t \neq \infty$. When $t \to \infty$, however, the free waves with σ_m will die away entirely.

Proudman's eq. (2.3) for semi-infinite canal does not correspond a motion started from rest a finite time before. It has a form similar to our eq. (44′a), which, when $t \to \infty$, holds good only for $\nu \equiv 0$, and if $\nu \neq 0$ however small, free oscillations will vanish for $t \to \infty$, as seen from (44a).

Net Densities and X-ray Investigation of Carbon

By Yoshiaki Matsunaga

(Received June, 12, 1935)

Abstract

Various kinds of sugar charcoals and pitch cokes, obtained by the carbonization or annealing at various temperatures and for various durations of time, were examined by measuring their net densities and by means of X-rays.

The question whether amorphous carbon represents a third modification of carbon or whether it is only finely divided graphite was first examined by P. Debye and P. Scherrer[1] by means of X-ray diffraction. All specimens were found to give diffraction patterns consisting of diffuse lines or bands. As the positions of the bands on the photograph were roughly indentical with those of certain lines of the graphite pattern, they concluded that the so-called amorphous carbon was nothing but graphite consisting of very fine crystallites. The next investigation on the same field was made by G. Asahara[2], who examined 35 different specimens of graphite and amorphous carbon by using tungsten radiation, and came to the same conclusion, viz., that amorphous carbon had the same lattice form as graphite and was not the third modification of carbon. Recently T. Watanabe[3] examined the carbon obtained from carbon monoxide; and Y. Oshima and Y. Fukuda[4] examined coke and charcoal by X-ray diffraction, coming to a similar conclusion. More recently M. Miwa[5] investigated various forms of carbon by means of cathode ray diffraction and agreed with the view that amorphous carbon was simply microcrystalline graphite.

Another group of investigators O. Ruff, Schmidt and Olbricht[6] inclined to the view that amorphous carbon was a "para-crystalline state" of matter bridging the amorphous and crystalline states more effectually than what is known as the "mesomorphic" or liquid crystal state. G. L. Clark[7] by means of the X-ray diffraction method and chemical considerations deduced the conclusion that the "para-crystalline state" actually existed. N. K. Chaney and his co-workers[8], from their investigations of the absorbing power of active carbon divided amorphous carbon into Alpha and Beta modifications. Recently P. Rishnamurti[9] and P. C. Mukherjee[10] examined sugar charcoal, an active

carbon and Ascheson graphite, by means of X-rays, and obtained the result that the lattice constant of the amorphous carbon was larger than that of ordinary graphite.

In the present investigation the writer measured the net densities of various carbons subjected to varied heat treatment, in parallel with the X-ray examination. It is most important that the material used in the experiments should be absolutely pure. Kahlbaum sugar which was first caramelled at 195°C. was put in a platinum crucible and was then charred in muffle electric furnace at various temperatures for 3 hours. The net densities of the fine powders of the specimens thus charred at various temperatures were measured by the method devised by U. Yoshida and B. Takei[11], which is especially suitable for obtaining net densities of porous and powdery substances. To get a general idea of the relation between the carbonizing temperature and the net densities, the results were plotted (Fig. 1), the net densities of carbon as ordinates, and the carbonizing temperatures as abscissae.

Table I

Graphite		Electrode Carbon					
		No. 1		No. 3		Carbonized at 880°C.	
θ (glancing angle)	Intensity	θ (glancing angle)	Intensity	θ (glancing angle)	Intensity	θ (glancing angle)	Intensity
6° 1′	W	6° 6′	W				
9° 36′	m						
10° 4′	S						
11° 21′	m	11° 19′	S	11° 19′	W	11° 9′	band S
12° 4′	S	12° 35′	S	12° 35′	S	↕	
13° 14′	S	13° 26′	S			13° 3′	
15° 30′	VW	15° 33′	VW	15° 33′	VW		
16° 46′	m	16° 48′	W				
17° 53′	S						
18° 4′	m						
18° 17′	m						
19° 43′	W	19° 20′	W	19° 20′	W		
20° 27′	VW						
20° 48′	VW	20° 47′	VW				
21° 53′	S	21° 43′	m	21° 43′	m	21° 12′	W
		24° 22′	m				
		26° 50′	W				

As is evident from the curve thus plotted, the net density of carbon increases as the carbonizing temperature is raised. With 250°C. charcoal (by which is meant charcoal carbonized at 250°C, a similar notation being employed for the higher carbonizing temperatures) and 300°C charcoal the presence of the sugar composition was tested by Fehling's solution, but no traces were found. On comparing the net densities of these two charcoals with that of 400°C. charcoal, a sudden increase with the carbonizing temperature was observed. This change, being very important, will be fully discussed later in conjunction with the results obtained from X-ray photographs.

In the same way the sugar charcoal (whose net density was 1.537) and pitch cokes (whose net density was 1.561) were annealed at various temperatures for 3 or 6 hours. The net densities of these specimens were also measured, and the relation between the annealing temperature and the net densities is also represented in Fig. 1.

It seems to be evident, from the curves thus drawn, that the net density of carbon annealed at a given temperature is only increased

Sugar charcoal

Carbonized at 400°C.		Carbonized at 350°C.		Carbonized at 290°C		Carbonized at 250°C.	
θ (glancing angle)	Intensity	θ (glancing angle)	Intensity	θ (glancing angle)	Intensity	θ (glancing angle)	Intensity
11° 9′ ↕ 13° 3′	band S	9° 45′ ↕ 13° 3′	band S	7° 53′ ↕ 10° 51′	band S	8° 21′ ↕ 9° 29′	band S
21° 12′	W	21°	VW				

very slightly with increase of the annealing time; and the net density of carbon annealed at a given temperature takes nearly a value which is characteristics of the annealing temperature. This fact means that the so-called "Graphitierungsgrad" is nearly a constant for a given annealing temperature.

Fig. 1

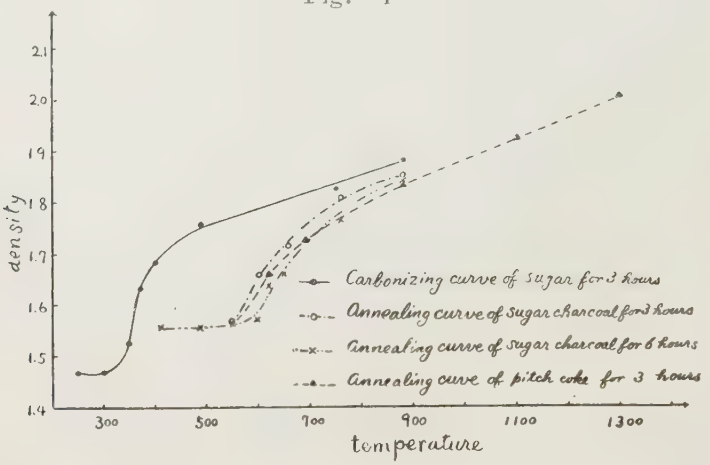

As is evident from the curves in Fig. I, the net density of the carbon prepared by carbonization increases very rapidly with the carbonizing temperature when the latter exceeds 350°C. approximately, and that of the specimen annealed also increases very rapidly when the annealing temperature is higher than about 600°C.

On the other hand, some of the specimens of known net densities were examined by means of X-rays generated from a Shearer tube having a copper target. The results obtained with various specimens are tabulated in Table I. In order to compare the quality of the electrode carbon two different specimens No. 1 (whose net density was 2.211) and No. 3 (whose net density was 2.069) which were annealed at about 2500°C. and 1400°C. respectively were also examined. The glancing angles θ measured on the photographs for various diffraction lines or bands are given in Table I. It is seen clearly, from the diffraction photographs, that the interference line become sharper as the net densities increase, and the smaller the net densities the more diffuse the lines. With the 250°C charcoal there could not be found any ordinary lines observed with the specimens carbonized at temperatures higher than 400°C., but only a diffuse band appeared at $\theta = 10^{\circ}$. Of course this small angle scattering also occured in the case of 880°C. and 400°C. charcoal.

Fig. 2

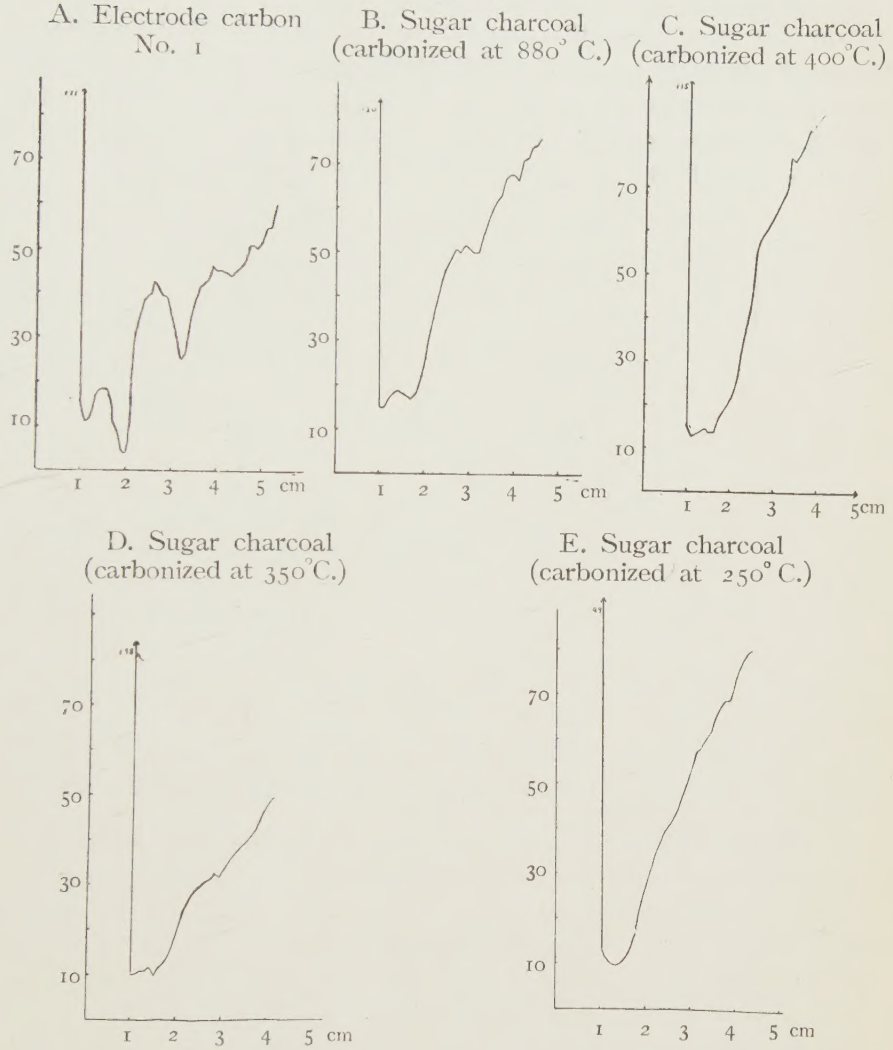
A. Electrode carbon No. 1
B. Sugar charcoal (carbonized at 880° C.)
C. Sugar charcoal (carbonized at 400°C.)
D. Sugar charcoal (carbonized at 350°C.)
E. Sugar charcoal (carbonized at 250° C.)
70
50
30
10
1 2 3 4 5 cm

Fig. 2 shows microphotometer records of some of the specimens. The difference in the X-ray photographs between 250°C. and 400°C. charcoal corresponds clearly to the difference in the net densities between the two. As already mentioned the 250°C charcoal was confirmed to contain no sugar composition by means of the Fehling's solution.

Thus it may be concluded that the net density of the so-called amorphous carbon (whether amorphous or fine crystalline state other

than graphite is undecided) is equal to 1.475 and that the ordinary carbon is a mixture of this amorphous carbon and graphite whose net density is equal to 2.268. The weight percentages of the graphite content in the mixtures are shown in Fig. 3. It will be clearly seen that these curves in Fig. 1 are similar to those of Fig. 3. This result agrees well with that obtained by the X-ray examination.

Fig. 3

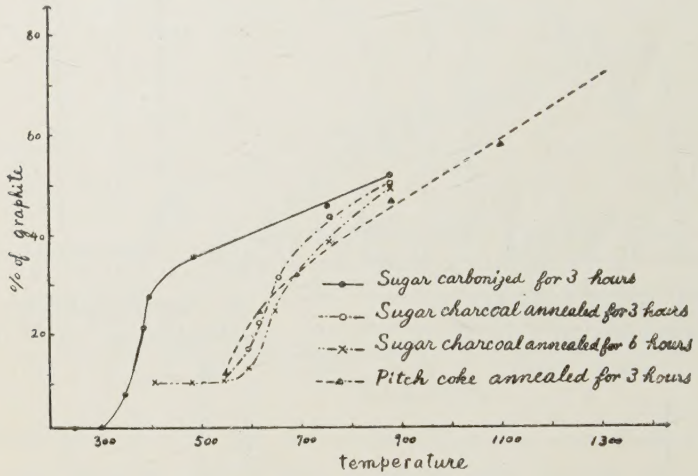

In conclusion, the writer wishes to express his sincere thanks to Prof. U. Yoshida for his kind guidance and invaluable suggestions.

Industrial Physical Laboratory, Nagoya Commercial College

(April 11, 1935)

References

1. P. Debye and S. P. Scherrer: Phys. Zeit., (1917) 301.
2. T. Asahara: Jap. Jour. Chem., **1** (1922) 35.
3. T. Watanabe: Sci. Pap. Inst. Phys. and Chem. Res., **8** (1929) 288.
4. Y. Oshima and Y. Fukuda: Jour. Soc. Chem. Ind., Jap., **32** (1929) 288.
5. M. Miwa: Sci. Rep. Tohoku Imp. Univ., **23** (1934) 242.
6. O. Ruff etc.: Zeit. Anorg. Allg. Chem., **148** (1925) 313.
7. G. L. Clark: Applied X-ray, (1927) 177.
8. N. K. Chaney: Trans. Amer. Electrochem. Soc., **36** (1919) 91.
9. P. K. Rishnamurti: Indian Jour. Phys., **61** (1930) 473.
10. P. C. Mukherjee: Zeit. Phys., **88** (1934) 247.
11. U. Yoshida and B. Takei: These Memoirs., **15** (1932) 1.

Vol. XVIII, No. 4, Published July 31, 1935

Price - - - - Yen 1.10

These Memoirs are on Sale at

MARUZEN COMPANY, LTD.

TOKYO, OSAKA, KYOTO, NAGOYA, YOKOHAMA,
FUKUOKA & SENDAI

昭和十年七月二十五日印刷
昭和十年七月三十一日發行

編纂兼發行者　京都帝國大學理學部

印刷者　須磨勘兵衞
京都市下京區北小路通新町西

印刷所　內外出版印刷株式會社
京都市下京區西洞院通七條南

賣捌所　丸善株式會社
東京、大阪、京都、名古屋、横濱、福岡、仙臺

CONTENTS

Net Density of Starch
By Bunsuke Takei 169
A Study of the Minor Fluctuation of the Atmospheric Pressure (III)
By Tadao Namekawa 173
A Theory of Tunamis and Seiches produced by Wind and Barometric Gradient
By Takaharu Nomitsu 201
Net Density and X-ray Investigation of Carbon
By Yoshiaki Matsunaga 215